A fluvial record of active fault-propagation folding, Salsomaggiore anticline, northern Apennines, Italy

Luke F. Wilson,[1,2] Frank J. Pazzaglia,[1] and David J. Anastasio[1]

Received 4 August 2008; revised 9 April 2009; accepted 27 May 2009; published 13 August 2009.

[1] Fault-propagation folds offer the potential to relate folding to underlying fault propagation and slip provided that fold kinematics can be established. Fluvial terraces have been recognized as kinematic indicators, but precise relationships between surface uplift and various folding mechanisms remain largely unexplored. This study takes advantage of a well-preserved, progressively deformed suite of middle Pleistocene to Recent fluvial terraces above a growing fault-propagation fold at the Apennine mountain front, northern Italy, to constrain the recent fold kinematics and place them in the context of a longer growth history gleaned from older growth strata. The geometry of straths and overlying terrace deposits defines a fixed anticlinal hinge, a rolling synclinal hinge, proxies for fault tip propagation rates, rock uplift rates, and tilting rates, and how these features and rates vary over the last ~800 ka along ~15 km of strike length. Field studies are augmented with DEM-based quantitative geomorphic analyses that document catchment hypsometry, mean anticlinal hinge elevation, and long profile form. Notably, long-term rock uplift rates (using incision as a proxy) are uniformly correlated with fault propagation and associated synclinal hinge migration, mean anticlinal hinge elevation and variations in catchment hypsometries. Channels that cross the forelimb at a high angle to the fold hinge generally have higher concavities, but channel steepness, commonly thought to reflect rock uplift, is more strongly adjusted to rock type. This study elucidates a new understanding of a complex fold growth history extending back at least 10 Ma and provides a novel demonstration of how fluvial terraces may be utilized to constrain fault-related fold kinematics.

Citation: Wilson, L. F., F. J. Pazzaglia, and D. J. Anastasio (2009), A fluvial record of active fault-propagation folding, Salsomaggiore anticline, northern Apennines, Italy, *J. Geophys. Res.*, *114*, B08403, doi:10.1029/2008JB005984.

1. Introduction

[2] Numerous theoretical models variably based on field and analog data have been developed over the past few decades to explain the kinematics of fault-related folding [e.g., *Suppe*, 1983, 1985; *Jamison*, 1987; *Mitra*, 1990; *Suppe and Medwedeff*, 1990; *Erslev*, 1991; *Hardy and Poblet*, 1994; *Allmendinger*, 1998; *Tavani et al.*, 2006; *Bernard et al.*, 2007]. Many studies have integrated these kinematic models with diachronous, incremental deformation markers such as growth strata [e.g., *Suppe et al.*, 1992] and fluvial terraces [e.g., *Rockwell et al.*, 1988; *Molnar et al.*, 1994; *Benedetti et al.*, 2000; *Lavé and Avouac*, 2000; *Thompson et al.*, 2002; *Gold et al.*, 2006; *Daëron et al.*, 2007; *Hubert-Ferrari et al.*, 2007; *Simoes et al.*, 2007; *Picotti and Pazzaglia*, 2008] to determine shortening and fault slip rates, important for seismic hazard assessment and our understanding of strain partitioning in space and time. These integrated studies are predicated on close agreement between the chosen kinematic model and the kinematics of the fold in question, which are typically difficult to confirm. Various approaches have been employed to confirm fault-related fold kinematics, including the distribution of mesoscopic deformation [e.g., *Fischer and Woodward*, 1992] and microscopic incremental strain markers [e.g., *Fisher and Anastasio*, 1994; *Anastasio et al.*, 1997], the geometry of growth strata [e.g., *Suppe et al.*, 1992; *Vergés et al.*, 1996; *Zapata and Allmendinger*, 1996; *Ford et al.*, 1997; *Storti and Poblet*, 1997; *Suppe et al.*, 1997; *Rafini and Mercier*, 2002], and geomorphic features such as terraced hillslopes [*Mueller and Suppe*, 1997; *Ahmadi et al.*, 2006]. Another approach is to use the geometry of fluvial terraces [*Gold et al.*, 2006; *Scharer et al.*, 2006].

[3] The use of fluvial terraces to constrain rock deformation is based on the premise that vertical channel incision is primarily a response to rock uplift, and other contributions to downcutting such as distal base-level fall and climatically modulated changes in watershed hydrology can be independently determined [e.g., *Rockwell et al.*, 1984; *Lavé and Avouac*, 2000]. In these settings, kinematic scenarios that result in different uplift patterns at the surface should be distinguishable using the geometry of fluvial terraces. Moreover, in this context, fluvial terraces are passive,

[1]Department of Earth and Environmental Sciences, Lehigh University, Bethlehem, Pennsylvania, USA.
[2]Now at ExxonMobil Exploration Company, Houston, Texas, USA.

0148-0227/09/2008JB005984$09.00

progressively formed, deformation markers and an updip, exposed extension of growth strata in actively subsiding basins (Figure 1). As such, the age and geometry of fluvial terraces can be used in the same manner that growth strata have previously been used to constrain deformation kinematics and rates [*Thompson et al.*, 2002; *Scharer et al.*, 2006; *Daëron et al.*, 2007].

[4] There are many advantages to using fluvial terraces over (or with) their downdip-equivalent, growth strata in the subsiding basin to constrain the kinematics of active structures [*Scharer et al.*, 2006]. First, fluvial terraces are generally much more accessible than growth strata in subsiding basins. Second, fluvial terraces are more commonly preserved above fold crests, where growth strata are often not developed or preserved. Third, the position of straths (unconformities at the base of fluvial terrace deposits) is generally not dictated by the amount of sedimentation that took place since the time of formation of the last unconformity. Fourth, terraces lack the nearly identical offlap geometries of some growth strata that make interpretation of the latter ambiguous [*Casas-Sainz et al.*, 2005]. Finally, even where terraces are not preserved as continuous features, their use as an uplift proxy is still useful because the distribution of the vertical velocity field can be used to constrain kinematics [*Hardy and Poblet*, 2005]. In sum, the geometry of fluvial terraces either combined with or independent of their associated deposits in the subsiding basin may result in fewer and less ambiguous solutions to the problem of relating geometry to kinematics.

[5] This study utilizes a suite of middle Pleistocene to Recent fluvial terraces preserved above the actively growing Salsomaggiore anticline in the northern Apennines, Italy. This is an outstanding locality for such a study because of the excellent preservation of multiple terrace deposits ranging in age from ~800 ka to Recent. Using incision as a direct proxy for uplift, the geometry and age of progressively deformed terraces are used to constrain the kinematics and rates of growth of the underlying fault-propagation fold. To better understand how terrace age and geometry relate to growth of the underlying anticline, we synthesize other surface and subsurface constraints on the geometry of the structure, the general earlier growth history that led to the present geometry, as well as the signature in the landscape of active deformation.

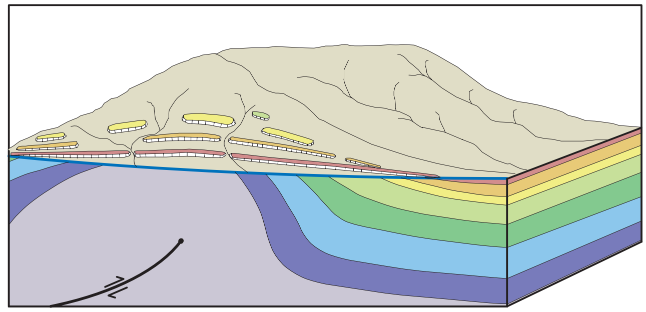

Figure 1. Schematic illustration showing how fluvial terraces that form above a growing fault-propagation fold may project downdip to growth strata in the actively subsiding basin. River profile is shown in blue. Growth strata in subsiding basins are generally time-correlative to straths formed in adjacent, uplifting regions.

2. Geologic Setting

[6] The Apennine Mountains of Italy are the subaerial expression of a collisional orogenic wedge that has developed since Oligocene time (~30 Ma) in the broader collision between Africa and Eurasia. Adria is a microplate of African affinity that has subducted since the Eocene [*Pieri and Mattavelli*, 1986] to build the Alps, Dinarides, and Apennines. Since the Oligocene, a north dipping Alpine subduction zone in the region of the modern western Mediterranean Sea has rotated counterclockwise about an Euler pole in central Europe to result in the modern, largely west dipping subduction zone beneath the Apennines (Figure 2a) [*Dewey et al.*, 1989]. As the Adriatic slab underwent rollback to the southeast and east, the Apennine orogenic wedge, marked by a leading edge, contractional fold-thrust belt and a trailing edge, extensional belt, migrated with the slab [e.g., *Malinverno and Ryan*, 1986]. The Apennines grew underwater throughout most of the Neogene and have become emergent largely within the last 1–2 million years.

[7] Oligocene to Messinian (~6 Ma) growth of the wedge was characterized by alternating underplating and frontal accretion of olistostromes, Adria crustal blocks, and deep-water turbidites with a largely Alpine provenance that were deposited in a trench (or foredeep) basin in front of the advancing wedge [e.g., *Ricci Lucchi*, 1975, 1986; *Pini*, 1999]. Oligocene-Miocene strata originally deposited on top of the downgoing Adriatic slab were accreted to the Apennine wedge. That accretionary part of the wedge is structurally overlain by the Ligurian "lid," a mélange composed of Jurassic-Paleogene remnants of oceanic crust that formed during Alpine and Eo-Alpine orogenesis and subsequently rifted off the southern Eurasian margin when backarc extension was initiated in late Oligocene time [*Pini*, 1999]. Middle-late Eocene to Pliocene Epiligurian marine sediments accumulated in piggyback/wedge-top basins atop the Ligurian lid [*Ori and Friend*, 1984; *Pini*, 1999]. The wedge experienced one or more brief periods (~5.96–5.33 Ma) of regional subaerial exposure and concomitant evaporite and nonmarine clastic sedimentation in the late Messinian due to partial desiccation of the Mediterranean Sea [e.g., *Manzi et al.*, 2005]; otherwise, it remained largely subaqueous until the Pleistocene. Topographic emergence of the Apennines has taken place as the wedge has overridden the thicker west facing passive margin of the Adriatic continental platform.

2.1. Northern Apennines Fold-Thrust Belt

[8] The thrust belt in the northern Apennines (Figure 2b) can be divided into a northwestern Emilia sector where the Ligurian lid is intact and a southeastern Romagna sector where the Ligurian lid has been eroded [e.g., *Zattin et al.*, 2002], separated by the northeast trending Sillaro Line southeast of the city of Bologna [e.g., *Artoni et al.*, 2004]. Growth of the Salsomaggiore anticline has created an erosional window through the Ligurian lid in the Emilia sector. The Emilia sector is commonly divided into three arcuate thrust systems: from west to east, the Monferrato

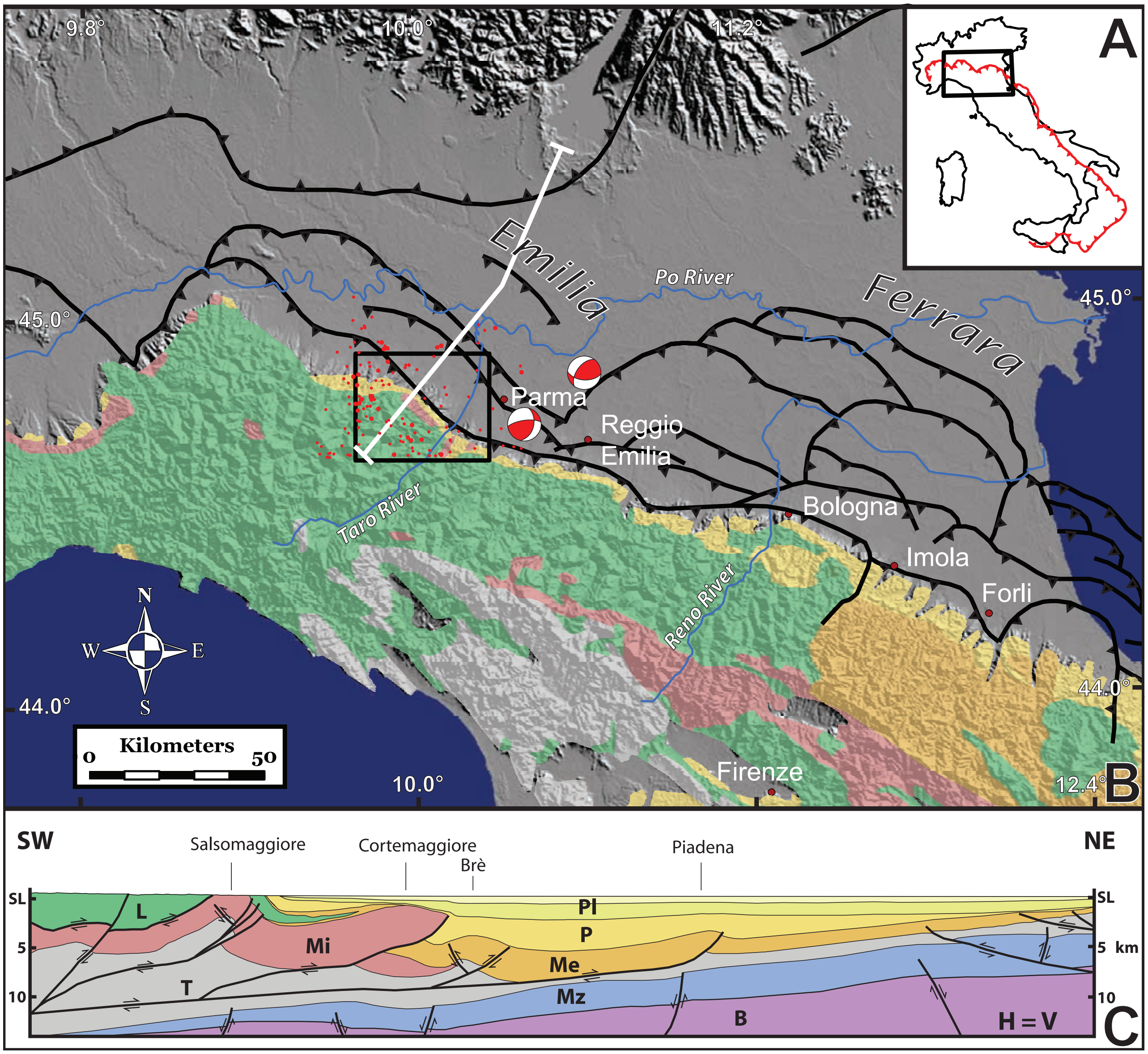

Figure 2. (a) Map of Italy showing outline of Figure 2b. The modern thrust front is shown in red [from *Bigi et al.*, 1990]. (b) Geologic map of the northern Apennines [modified from *Bigi et al.*, 1990]. Major thrusts buried beneath the Po Plain are shown. Colors correspond to units shown in Figure 2c. Microseismicity (M = 1.6–4.3) at 1–15 km depths from 1981 to 2002 is shown with red dots (from the Italian Seismic Catalog). Oblique thrust focal mechanisms for the 1983 Parma (M = 5.0) and 1996 Reggio Emilia (M = 5.4) earthquakes are from the Harvard Centroid Moment Tensor Catalog. Some of the major cities, rivers, and the Ferrara and Emilia arcs are labeled. The box around the Salsomaggiore anticline shows the spatial extent of Figures 3, 4, 8a, 9b, 10, and 11. (c) Cross section across the Salsomaggiore anticline and buried thrust belt (line of section shown in Figure 2b), based on an AGIP seismic line [*Pieri*, 1983], well data, and cross sections by *Pieri* [1992] and *Picotti et al.* [2007]. Depth to basement is constrained by gravity and magnetic data. L, Ligurian; B, pre-Mesozoic basement; Mz, Mesozoic, undivided; T, Tertiary, undivided; Mi, Langhian-Tortonian; Me, Messinian; P, Pliocene; Pl, Pleistocene-Holocene.

Arc, the Emilia Arc, and the Ferrara arc, the frontal most parts of which are buried and largely inactive beneath the Po foreland. Deformation is thought to have initiated at progressively later times toward the east, beginning in the early Miocene at the Monferrato arc, the Tortonian at the Emilia arc, and the early Pliocene at the Ferrara arc [*Castellarin and Vai*, 1986]. The Salsomaggiore anticline, cored by the Salsomaggiore thrust, resides in the Emilia arc at the topographic range front but 20 and 45 km from the more fontal Cortemaggiore and Piadena thrusts, respectively (Figure 2c). *Picotti et al.* [2007] estimate a total of 6 km of shortening accommodated by the Salsomaggiore structure and 7 km by the Cortemaggiore structure.

2.2. Salsomaggiore Anticline

[9] The Salsomaggiore anticline is named after the town of Salsomaggiore in the Ghiara valley (Figure 3). The core of the anticline exposed at the surface is composed of Langhian and Serravallian strata, the back limb includes Aquitanian-Burdigalian, Epiligurian deposits, and outcropping on the forelimb are Messinian-Recent strata with shallowing upward dips (Figure 3). The anticline is elongate and doubly plunging with a domal crest located near the town of Tabiano. The main anticlinal axis trends northwest-southeast, the tightness of the fold varies along strike and is asymmetric, with a slightly overturned forelimb (in the subsurface) [e.g., *Di Dio et al.*, 2005] at the strike of the Rio Gisolo (Parola catchment, Figure 3). At the surface, Messinian strata have an average dip of 30 degrees in the Stirone valley, 60 degrees near the Parola valley, and 50 degrees further southeast toward the west side of the Taro valley. In contrast, Pliocene strata generally dip 10–30 degrees in the Stirone and Parola valleys but as much as 45 degrees [*Di Dio et al.*, 2005] near the west side of the Taro valley. No major faults are exposed at the surface, but a well near the town of Salsomaggiore intersects two thrust imbricates and seismic data suggest a third and more significant thrust (the Salsomaggiore thrust) offsets Miocene strata on the forelimb at depth (Figure 2c) [*Picotti et al.*, 2007].

2.3. Salsomaggiore Stratigraphy

[10] The early and middle Miocene stratigraphy near Salsomaggiore includes Burdigalian deep-marine marls (Bisciaro Formation) overlain by Burdigalian-Langhian interbedded marls and sandstones (Torrente Ghiara Formation), Langhian marls (the Salsomaggiore marls, upper Torrente Ghiara Formation), and a Serravallian, coarsening upward succession of marls, sandstones, and conglomerates (Rio Gisolo Formation; Figure 3) [*Conti et al.*, 2007; *Picotti et al.*, 2007]. The Rio Gisolo Formation is unconformably overlain by the ''intra-Messinian chaotic unit'' (IMCU) [*Artoni et al.*, 2004], remnants (including kilometer size blocks) of the Ligurian lid, thought to have slumped off the toe of the main Ligurian deposit during the Messinian in a catastrophic mass wasting event with a breakaway zone located directly west of the Salsomaggiore anticline. The Torrente Ghiara, Rio Gisolo, and IMCU are overlain in angular unconformity by the Colombacci Formation, largely comprised in the Salsomaggiore area of fluviodeltaic strata deposited after the Mediterranean desiccation event [*Artoni*, 2003; *Artoni et al.*, 2007]. The Colombacci Formation is disconformably overlain by the Argille di Lugagnano Formation, which consists of lower to middle Pliocene, deep- to shallow-marine, gray-blue clays with subordinate fossiliferous silstones and calcarenites [e.g., *Channell et al.*, 1994]. Stratigraphically above the Argille di Lugagnano Formation are the upper Pliocene-lower Pleistocene, marginal marine Torrente Stirone and Costamezzana Formations [e.g., *Amorosi et al.*, 1998a; *Dominici*, 2001; *Di Dio et al.*, 2005] (Figure A1). Unconformably overlying the Costamezzana Formation is the oldest, significant, Pleistocene, continental deposit of widespread occurrence across the northern Apennines, R.E.R. unit AEI (Sintema Emiliano-Romagnolo Inferiore) [e.g., *Di Dio et al.*, 2005], which consists of fluviolacustrine sediments of middle Pleistocene age with abundant non-marine mollusks [e.g., *Pelosio and Raffi*, 1977; *Cremaschi*, 1982; *Ciangherotti et al.*, 1997]. Overlying AEI are alluvial deposits and related fluvial terraces of the Sintema Emiliano-Romagnolo Superiore (AES) [*Di Dio et al.*, 2005] that are the focus of this study.

2.4. Miocene–Early Pleistocene Growth

[11] *Castellarin and Vai* [1986] suggest that formation of the Emilia thrust system occurred during the Tortonian, consistent with the initiation of major extension and opening of the northern Tyrrhenian Sea [*Rosenbaum and Lister*, 2004]. Major Tortonian growth of the Salsomaggiore anticline is suggested by a lack of Tortonian strata at the fold crest, but thick Tortonian strata in the subsurface on the forelimb and in the footwall of the Salsomaggiore thrust [*Picotti et al.*, 2007]. *Conti et al.* [2007] suggest the Salsomaggiore anticline was active and topographically elevated during the Serravallian, and this resulted in the coarsening upward succession of Serravallian strata now exposed on the back limb of the anticline. Even older fold growth in the Langhian [*Picotti et al.*, 2007] may be suggested by a local change in the clastic routing system: specifically, deactivation of a turbiditic lobe, manifested by the lack of interbedded sandstone in the upper Torrente Ghiara Formation (the Salsomaggiore marls). *Odin et al.* [1997] dated a volcanic ash layer within the Epiligurian succession on the backlimb of the anticline to be 18.4 ± 0.3 Ma (Ar-Ar total gas, $\pm 2\sigma$), suggesting an even older age of initial fold growth because deformation in the Ligurian lid is known to be linked to deformation in the underyling, accreted rocks [*Pini*, 1999]; the existence of an Epiligurian, wedge top basin bound by the modern Salsomaggiore anticline suggests the anticline was active when the wedge top basin formed. However, the wedge top basin could have formed at a more hinterward location and been subsequently transported toward the Salsomaggiore anticline. Regardless of exactly when growth of the structure was initiated, significant growth probably did not begin until the Tortonian.

[12] Convergence of seismic reflectors on the back limb of the Cortemaggiore anticline, displayed on a published AGIP seismic section [*Pieri*, 1983] suggests that most contractional deformation stepped inboard to the adjacent Cortemaggiore thrust by the end of the Tortonian [*Artoni et al.*, 2007; *Picotti et al.*, 2007]. The cross section trending parallel to the main anticlinal axis published by *Picotti et al.* [2007], constrained by seismic and well data, shows the Salsomaggiore thrust and the immediate hanging wall and footwall are folded above the Cortemaggiore thrust, which is a lateral ramp beneath the Salsomaggiore anticline. Fault-bend folding over this deeper lateral ramp is manifest at the surface in bedding attitudes and the map pattern as a

Figure 3. Local bedrock geologic map modified from the Regione Emilia Romagna (R.E.R.) geological survey, draped over 10 m DEM hill shade. Major streams are labeled. The timescale is from *Gradstein et al.* [2004], and the ages of the units are described in the text. The Taro River was digitized from 1:10,000 topographic maps.

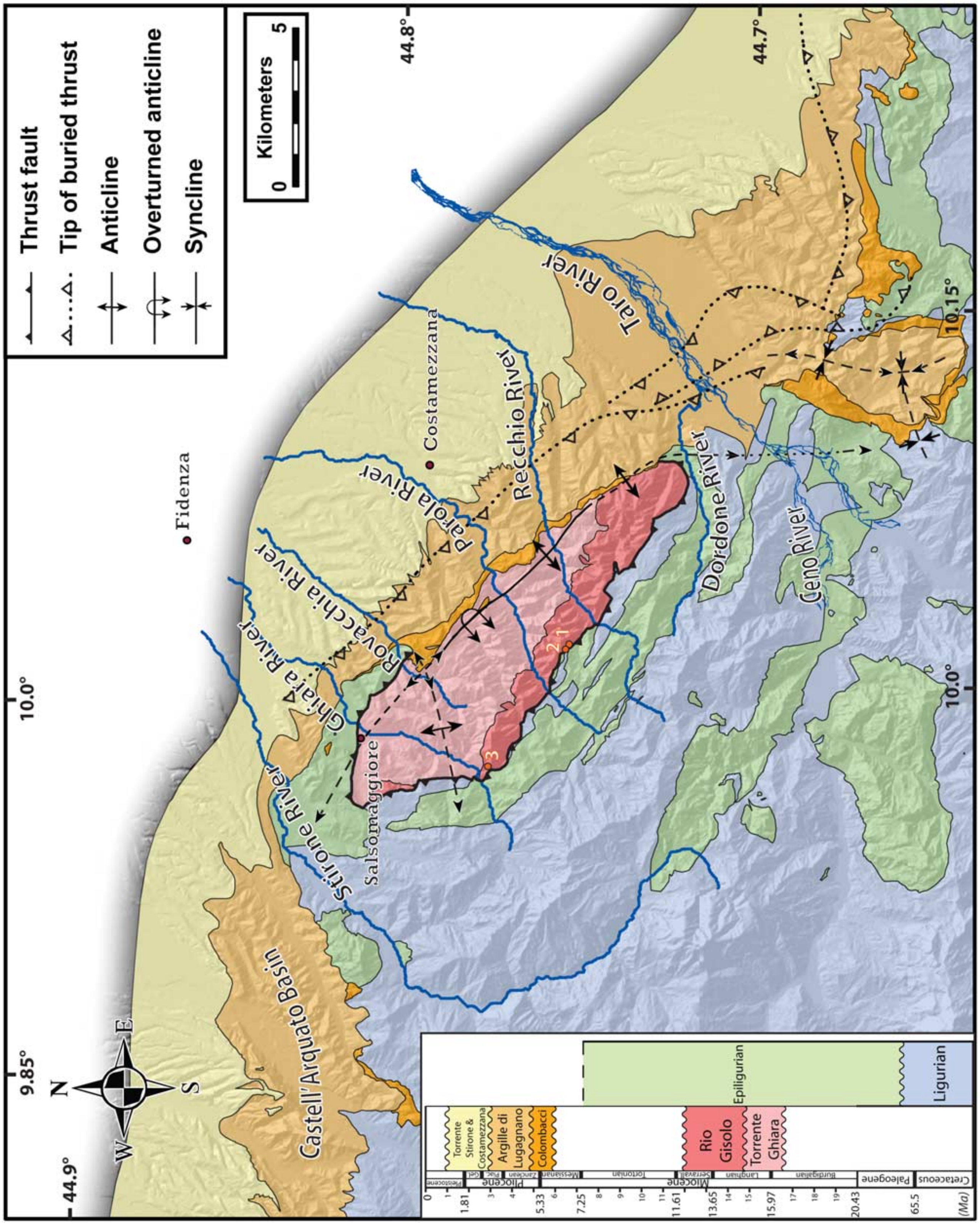
Thrust fault
Tip of buried thrust
Anticline
Overturned anticline
Syncline
Kilometers
0
5
44.8°
44.7°
44.9°
9.85°
10.0°
10.15°
N
S
E
W
Taro River
Recchio River
Parola River
Rovacchia River
Ghiara River
Stirone River
Dordone River
Ceno River
Costamezzana
Fidenza
Salsomaggiore
Castell'Arquato Basin
Torrente Stirone & Costamezzana
Argille di Lugagnano
Colombacci
Rio Gisolo
Torrente Ghiara
Epiligurian
Ligurian
Pleistocene
Pliocene
Miocene
Paleogene
Cretaceous
Messinian
Tortonian
Serravallian
Langhian
Burdigalian
1.81
5.33
7.25
11.61
13.65
15.97
20.43
65.5
(Ma)

Figure 3

transverse anticlinal hinge. The thickness of exposed Serravallian strata on the back limb of the anticline decreases to zero approaching the transverse hinge and thickens in the upper Ghiara catchment on the opposite limb (Figure 3). These observations suggest that following major Tortonian growth, the Salsomaggiore anticline became a dome-shaped fold due to slip on the underlying Cortemaggiore thrust.

[13] Precisely when oblique slip on the Cortemaggiore lateral ramp resulted in overlying fold interference is partly constrained by chronostratigraphy. Folding of lower Pleistocene strata on the AGIP seismic line interpreted by *Pieri* [1983], *Di Dio et al.* [1997], and *Picotti et al.* [2007] suggests that growth of the Cortemaggiore anticline persisted until the early Pleistocene, so cross folding could have occurred anytime between the end of the Tortonian and the early Pleistocene. However, the variation in age of Pliocene strata along strike of the Salsomaggiore anticline suggests that most of this deformation occurred during the Pliocene. Particularly revealing are Pliocene strata in the Castell' Arquato Basin (CAB) and the Stirone catchment (Figure 3). The recently published stratigraphic model of the CAB by *Roveri and Taviani* [2003], which was based on magnetostratigraphy and biostratigraphy from numerous published and unpublished studies, shows a thick Pliocene succession spanning 1.5 million years ($\sim$4.2–2.7 Ma) in the CAB is time-correlative to a condensed section exposed along the Stirone river banks [also discussed by *Channell et al.*, 1994]. Thick accumulation of Pliocene strata at the location of the Stirone River proceeded after $\sim$2.7 Ma [e.g., *Mary et al.*, 1993]. The condensed Stirone section is likely a result of reduced accommodation associated with uplift during oblique slip on the Cortemaggiore lateral ramp. After the Salsomaggiore thrust was folded, slip was likely impeded, causing the successive formation of two unfolded, leading edge imbricate thrusts during continued shortening (Figure 2c).

[14] Growth of the Cortemaggiore anticline, as well as other structures in the subsurface of the modern Po Plain effectively ceased in the early Pleistocene, and the active deformation front stepped back to the location of the modern range front. The Salsomaggiore anticline was probably emergent during the early Pleistocene, based on onlap geometries of lower Pleistocene strata in the subsurface [*Dominici*, 2001]. Growth of the Salsomaggiore anticline above the unfolded thrust imbricates since early middle Pleistocene time is recorded by the fluvial terrace record.

3. Methods

3.1. Fluvial Terraces

[15] Fluvial terraces are both landforms and allostratigraphic units composed of alluvial deposits and created by unsteadiness in catchment sediment flux and channel incision. Terrace deposits are typically sand and gravel channel facies overlain by finer-grained overbank facies bound by basal strath and upper tread unconformities. The degree of pedogenic alteration of terrace deposits is a crude measure of tread stability and time since terrace genesis. Multiple pedogenic features were used as a proxy for terrace age and correlation, including degree of horizonization, accumulation of soluble salts such as calcium carbonate, degree of oxidation and rubification, and weathering rind thickness on gravel clasts [e.g., *Eppes et al.*, 2008]. Treads are also affected by poststabilization colluvial and alluvial fan deposition as well as fluvial dissection, both of which contribute to a suite of morphologic characteristics used to distinguish and correlate terraces. Utilizing these features, fluvial terrace deposits were mapped on a 1:10,000 scale topographic base in the field from late April to early June 2007. Mapping focused in three valleys that trend transverse to the main anticline axis and cover the breadth of the anticline: (from northwest to southeast) the Stirone, Parola, and Taro valleys (see Figure 3 for location). These detailed maps were integrated with a map published by R.E.R. [*Di Dio et al.*, 2005], which was field checked where possible, to produce a composite fluvial terrace map.

[16] The numeric age of a strath is constrained by dating the directly overlying terrace deposit, which must have been emplaced after or simultaneous to strath carving. Where terrace deposits are thin ($\sim$1–3 m) or nonexistent (a.k.a. a strath terrace) [*Bull*, 1991], it is reasonable to assume that the deposit represents the bed load of the stream at the time of strath carving, so the deposit and the strath are the same age [e.g., *Hancock and Anderson*, 2002]. Where terrace deposits are thicker (a.k.a. a fill terrace) [*Bull*, 1991] and document aggradation above the strath prior to rapid downcutting and terrace formation, the age of the base of the terrace deposit is the most accurate constraint on strath age. At Salsomaggiore, young terrace straths were dated by radiocarbon analyses of freshwater gastropod and bivalve shell fragments contained in the overlying terrace deposit, while older strath ages were constrained by pedogenic and surface morphologic correlation to terraces of known age in the nearby Reno valley (Figure 2b) [*Picotti and Pazzaglia*, 2008].

[17] Wide straths are particularly useful in active tectonic analyses. These straths are carved when rivers widen their valley bottoms through lateral corrasion, and are abandoned during periods of vertical incision [*Gilbert*, 1877; *Hancock and Anderson*, 2002]. The trade-off between lateral corrasion and vertical incision depends on the dynamic balance between sediment load and caliber, discharge, and channel slope [*Mackin*, 1937; *Schumm*, 1969]. Base-level changes, especially for streams near sea level, can have a significant effect on channel slope. Unsteadiness in sediment and water inputs to the fluvial system, are controlled mainly by changes in climate and the associated interactions with weathering processes, vegetation, bedrock lithology, and hillslope sediment transport [e.g., *Schumm*, 1969; *Bull*, 1991; *Pazzaglia and Gardner*, 1993; *Merritts et al.*, 1994; *Meyer et al.*, 1995; *Krzyszkowski*, 1996; *Amorosi et al.*, 2002; *Wegmann and Pazzaglia*, 2002; *Wegmann and Pazzaglia*, 2009]. A widely observed phenomenon is that during cold glacial times, there is less vegetation stabilizing hillslopes and increased sediment supply to channels, causing channels to aggrade [e.g., *Bull*, 1991; *Wegmann and Pazzaglia*, 2002]. Conversely, during warmer interglacial times, there is more vegetation stabilizing hillslopes and decreased sediment supply to channels, causing incision and terrace formation. Importantly, regardless of the specific details of channel response through time, once a strath and its alluvial cover are preserved in a region of active uplift they become a passive marker of rock deformation.

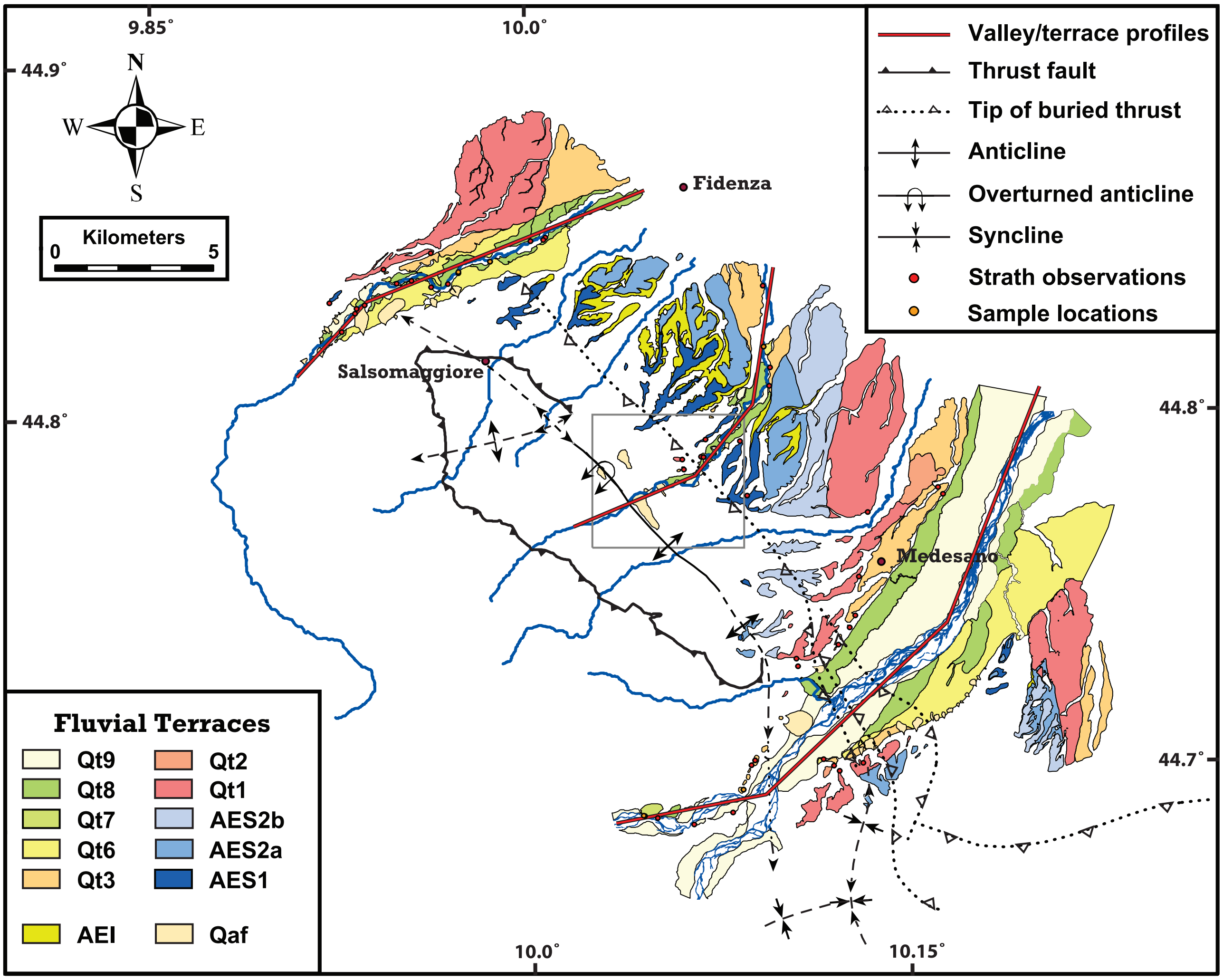

Figure 4. Fluvial terrace map. AES1 and AES2 are partially compiled from R.E.R. Wherever possible, straths were located in the field, and contacts on the map reflect known or estimated strath locations. Streams are labeled in Figure 3. Valley/terrace profile lines shown here are displayed in Figure 6. AES1-Qt1 between the Taro and Stirone valleys have a map pattern consistent with genetic association to the Taro River. The box in the center denotes the outline of Figure 12a.

[18] For the purpose of constraining rock deformation using fluvial terraces, straths are the preferred geometric element to characterize because the overlying deposit and tread are usually of variable thickness and modified by varying degrees of incision, alluvial fan deposition, and colluviation. In order to determine the finite deformation recorded by a strath, the original geometry must be known and is typically assumed to have the same geometry as the modern valley profile [e.g., *Pazzaglia and Brandon*, 2001], implying a long-term steady state. Because old straths have subsided below modern valley profiles approaching the Po foreland from the mountain front and we do not have accurate constraints on subsurface strath geometries, subaerially exposed strath elevations were compared to modern valley profile elevations as a proxy for rock uplift. Even though preserved straths are passive markers of rock deformation, because the datum to which they are referenced in this study is the modern valley profile, measurements of strath separations from modern stream channels are direct indicators of incision, and not necessarily uplift. However, incision generally balances rock uplift when integrated across at least one glacial cycle [*Pazzaglia and Brandon*, 2001], especially when streams are located at or near sea level, which is the case for the streams traversing the Salsomaggiore anticline. Therefore, the amount of incision recorded by straths older than ~100 ka referenced to modern valley bottoms should accurately reflect variations in underlying rock uplift.

[19] We do not contend in this study for the absence of isostatic uplift due to erosional unloading, or flexural uplift associated with sediment loading in the adjacent Po Plain. Rather, owing to the limited area considered in this study, any regional uplift unrelated to the local fault-related fold can be assumed uniform, so variations in uplift related to the underlying, growing fault-propagation fold should be reflected in the river incision. The difference between strath elevation and modern valley bottom elevation was measured using a digital barometric altimeter (accurate to 1–2 m). Modern valley bottom strath profiles were constructed from 1:10,000 topographic maps by projecting stream

elevations at 5 m contours to a straight profile that trends down the center of the valley. Measured vertical separations between straths and modern valley bottoms were then plotted above the valley profile to constrain strath profiles.

3.2. Topographic Metrics

[20] Topographic metrics were extracted from a 10 m digital elevation model in order to determine topographic fingerprints of underlying fold growth and consistencies with the fluvial terrace record. Analyzed metrics include catchment hypsometry, mean anticlinal hinge elevation, channel concavity, and channel steepness index.

[21] Catchment hypsometry was determined by binning elevations of pixels in each drainage area into twenty equal intervals, and then examining the frequency distribution of those pixels. Rather than constructing traditional (a/A versus h/H) hypsometric plots with the *x* axis representing cumulative area, h/H was plotted versus noncumulative, relative area percent of the catchment because these plots more clearly illustrate differences in hypsometry between catchments. The area percent is still relative (normalized) to the total area of that catchment, so catchments are still comparable regardless of size and absolute elevation. A swath topographic profile 0.5 km wide, centered on and paralleling the anticlinal hinge was constructed as another means of assessing along-strike variations in elevation that may reflect underlying fold growth. The swath profile was constructed by obtaining eleven parallel topographic profiles spaced 50 m apart, using Easy Profiler and a 10 m digital elevation model (DEM) in ArcGIS. Channel concavities (θ) and steepness indices (k_{sn}) were calculated using the Arcmap toolbar and Matlab script Profiler 5.1 (K. Whipple et al., New tools for quantitative geomorphology: Extraction and interpretation of stream profiles from digital topographic data, Geological Society of America Short Course, Boulder, Colorado, available at www.geomorph-tools.org, 2007). Previous work has shown that for equilibrium channel profiles of similar θ, k_{sn} should reflect rock uplift [*Snyder et al.*, 2000; *Duvall et al.*, 2004], and if channels in different locations are referenced to the same concavity, steepness indices should be comparable between those channels. Channel concavity is commonly thought to be relatively constant across diverse tectonic settings, though some studies have highlighted distinct changes in concavity associated with variable uplift rate [*Kirby and Whipple*, 2001], climate [*Zaprowski et al.*, 2005], and rock type [*Spagnolo and Pazzaglia*, 2005].

4. Results

4.1. Terrace Deposits: Map, Description, and Age

[22] Nine terrace deposits were mapped (Figure 4) and consist primarily of variably unconsolidated channel gravel with lesser amounts of sand and overbank mud. The naming scheme used (Figure 5) is adapted from two previous studies: *Di Dio et al.* [2005] and *Picotti and Pazzaglia* [2008]. The youngest six terrace deposits are given the same name as time-correlative terraces in the Reno valley mapped by *Picotti and Pazzaglia* [2008], while the oldest three terrace deposits are given names derived from a stratigraphy proposed by *Di Dio et al.* [2005] (most recent naming scheme of the geological survey of the R.E.R). Generally, these deposits thicken from ~1–3 m upstream of the mountain front (where they are designated Qt) to 10 or more meters toward the Po foreland (where they are designated Qa if they are not associated with a terrace landform).

[23] Four Holocene-late Pleistocene terraces (Qt6, Qt7, Qt8, and Qt9) are preserved in the modern valleys astride the Stirone, Parola, and Taro channels. Qt6 is the widest terrace in the Stirone valley and on the east side of the Taro valley, whereas Qt8 and Qt9 dominate the floor of the comparatively narrower Parola valley. The Qt6 deposit is generally thin (1–2 m), consisting entirely of gravel, and capped by a soil with a moderately developed (stage I+ to II−) calcic B-horizon. Qt7 is preserved in only one location above the Ceno River, directly upstream from the Taro river confluence. The tread of this terrace is covered by roads and buildings and there are no good exposures of the soil; however, an exposure on a cliff above the Ceno River reveals at least six meters of stratified gravel. In contrast, both Qt8 and Qt9 (Figure A1) are underlain by thin (1–2 m), stratified, sandy gravel and capped locally by a 0.5 m thick sandy-silt overbank deposit. Soils are weakly developed in these two terrace deposits and locally exhibit a stage I− calcic horizon. In the Taro valley, Qt9 has a gently corrugated tread consistent with gravel bar and swale topography.

[24] Qt7, Qt8, and Qt9 are dated by three new radiocarbon analyses of freshwater gastropod and bivalve shell fragments extracted from the terrace deposits (Table 1). The samples were collected from within ~1 m of the Qt8 and Qt9 straths and from the middle part of the thicker Qt7 deposit. The three dates from Qt7–9 overlap dates for terraces in similar landscape position in the Romagna and Marche Apennines [*Picotti and Pazzaglia*, 2008; *Wegmann and Pazzaglia*, 2009]. By extension, Qt6 and older terrace ages are assigned by comparing their soils and landscape position to dated terraces in the Reno valley (Figure 5) [*Picotti and Pazzaglia*, 2008].

[25] Other late Pleistocene terraces that are prominent above Emilia-Romagna Rivers (Qt4 and Qt5) are not present in the Salsomaggiore area; however, terraces representing middle Pleistocene or older valleys (Qt3, Qt2, and Qt1) are typically well preserved. In the Stirone and Taro valleys, Qt3 is a wide terrace underlain by a stratified, trough cross-bedded, gravelly sand and gravel, channel facies 2–4 m thick. In the Parola valley, Qt3 consists of brown-orange, semiconsolidated, gravel up to 10 m thick. The Qt3 soil is ~1 m thick, distinctly tan-orange colored, and contains abundant, conspicuous Fe-Mn pellets up to 1 cm across. Qt2 is mapped in two locations on the west side of the Taro valley, but no good exposures or soils of this terrace are preserved. Qt1 is underlain by thick (at least 6 m), gray, stratified, sandy gravel with local, cross-stratified, brown-gray sand. The Qt1/Qa1 deposit is well preserved in the Taro valley where a recent excavation near Medesano shows that it is capped by a very well developed, 2 m thick, clay-rich, red soil. This paleosol is buried downstream of Medesano by the Qt3 terrace.

[26] The Qt1 and Qt3 soils are very distinct and permit confident correlation to terraces dated elsewhere in the northern Apennines. The ages of Qt1, Qt2, and Qt3 in the Reno valley have been determined by projection of terraces into the subsurface of the Po Plain, where cyclic lithofacies

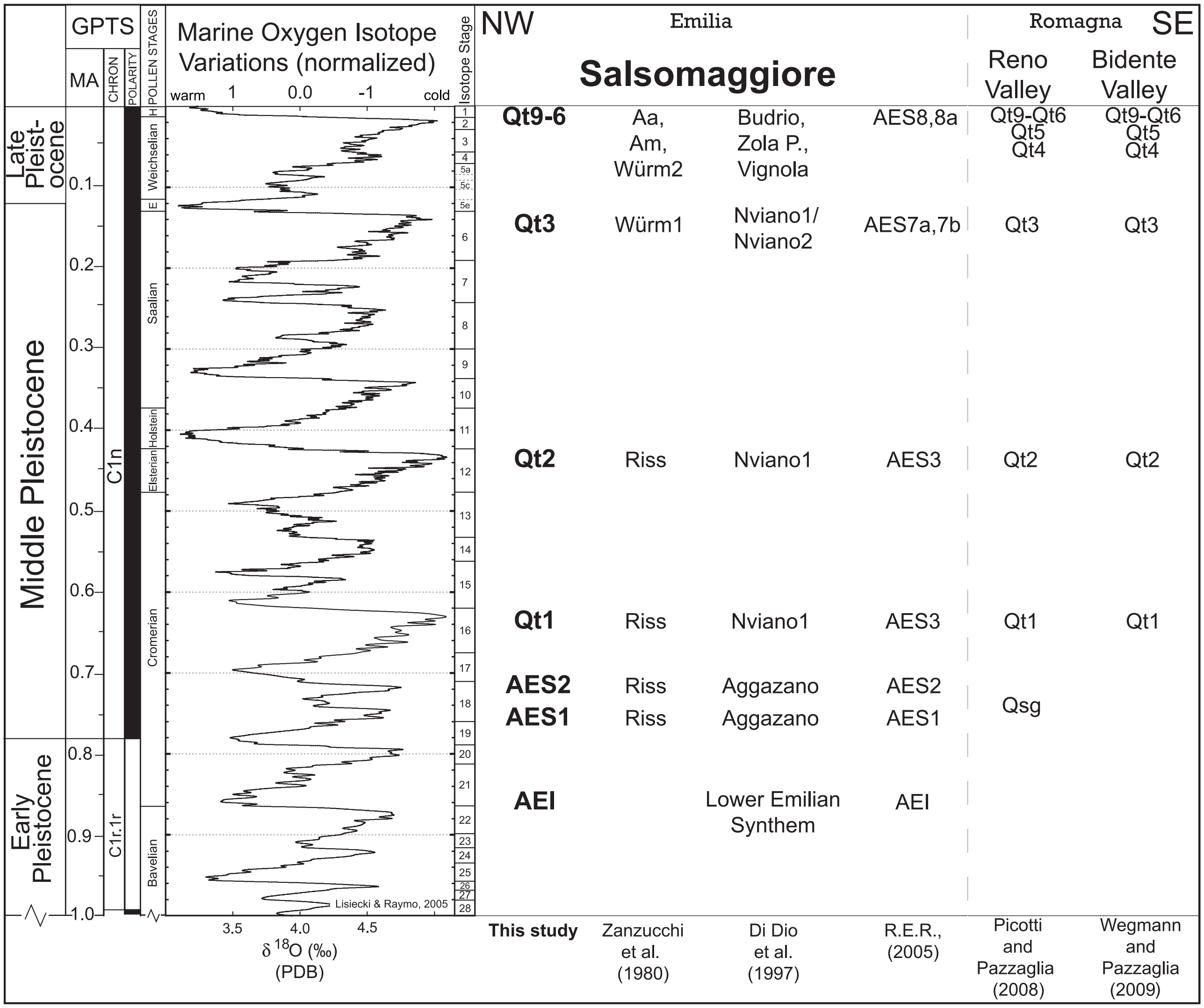

Figure 5. Fluvial terraces in this study are correlated to those previously mapped at Salsomaggiore and to those mapped in the Reno and Bidente valleys to the southeast in the Romagna Apennines. The ages of Qt1–Qt3 are constrained by tuning correlative, downdip strata in the adjacent basin to climate changes [*Picotti and Pazzaglia*, 2008], for which marine oxygen isotope records are a proxy and shown on the left.

and pollen assemblages are recorded in well logs and dated by calibration to glacial-interglacial climate cycles [*Amorosi et al.*, 1996, 2002; *Picotti and Pazzaglia*, 2008] of 620 ± 30, 440 ± 20, and 140 ± 10 ka, respectively.

[27] Terraces older than Qt1 mapped by *Picotti and Pazzaglia* [2008] are present at higher elevations than Qt1 outside of the context of the modern river valleys in the Salsomaggiore area and are designated AES1 and AES2a/2b. These deposits both consist mainly of red to maroon, semiconsolidated to indurated, clast-supported, pebble to small boulder conglomerate, and no distinct soil horizons were recognized in the field. Both units are particularly indurated where they are well exposed above the banks of the Parola River. The majority of the AES1 and AES2a/2b deposits mapped reside west of the modern Taro valley and appear genetically related to the Taro River because the map extent of these and successively younger terrace deposits gradually takes on the form of the modern Taro valley (Figure 4).

[28] AES1 and AES2a/2b are younger than the well-known AEI unit [*Di Dio et al.*, 2005], which does not have a preserved, updip terrace deposit. The base of the AEI deposit is magnetically reversed in the Stirone valley, meaning it is older than 780 ka [*Di Dio et al.*, 1997], but

Table 1. Results From Five Radiocarbon Analyses[a]

Sample	Terrace	^{14}C age (BP) ± 1σ	Calibrated Age (BP) ± 1σ
07-May29-1	Colluvium overlying Qt3	320 ± 45	376 ± 67
07-May31-1	Qt9	1785 ± 15	1707 ± 20
07-May25-2	Qt8	3200 ± 15	3413 ± 19
07-May30-2	Qt7	9130 ± 70	10271 ± 71
07-May22-7	Qt6	NA	NA

[a]Calibrated ages were calculated using the conversion of *Fairbanks et al.* [2005, and references within]. Sample locations are shown in Figure 4. Sample 07-May29-1 was dated to verify a Qt3 terrace deposit was radiocarbon dead, but the shells extracted apparently came from young snails that had burrowed into the deposit. Sample 07-May22-7 contained insufficient material for dating after the cleaning procedure.

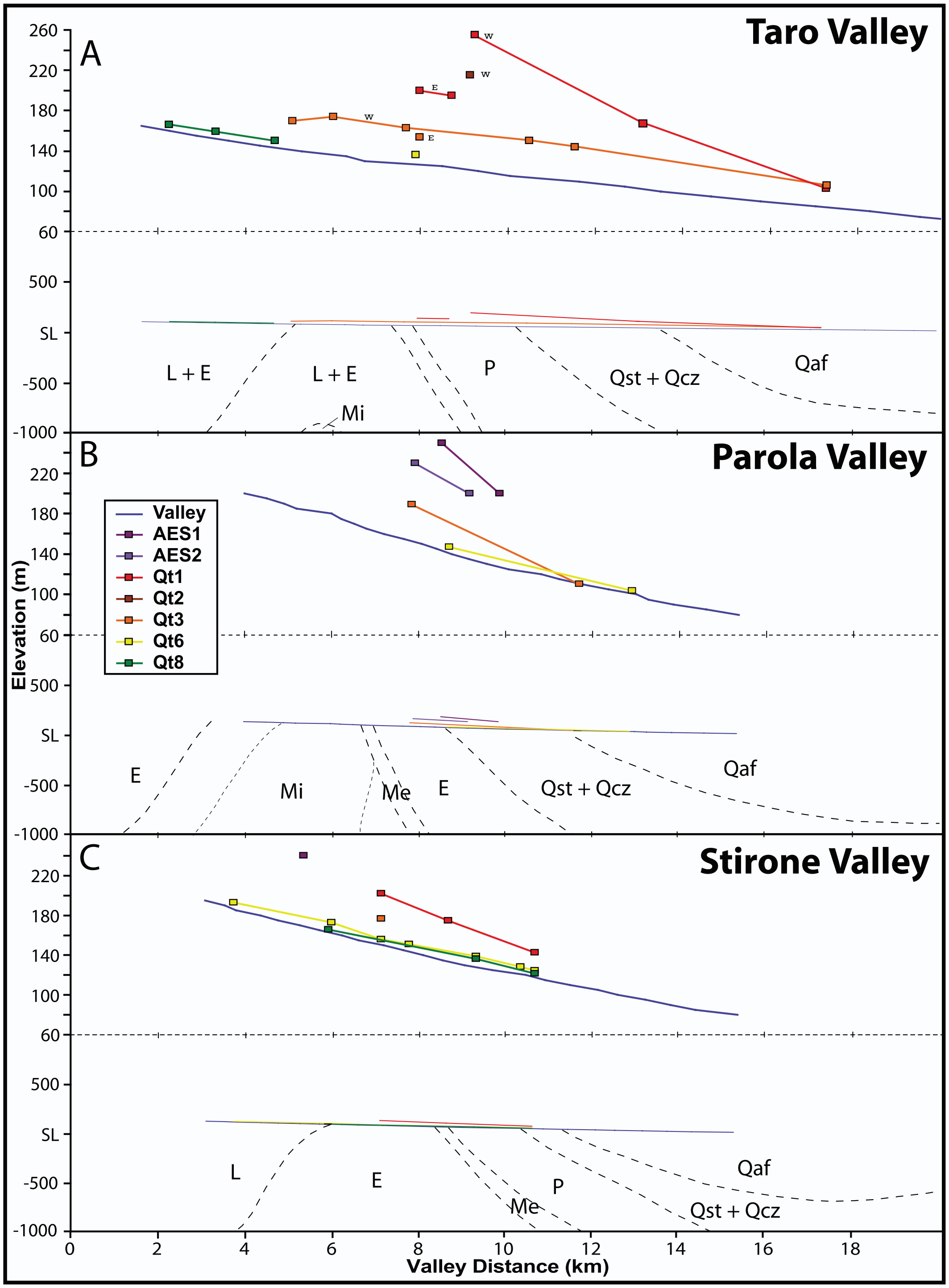

Figure 6. Measured strath elevations are plotted above profiles of the modern (a) Taro, (b) Parola, and (c) Stirone valley bottoms. Point measurements were connected with straight lines to aid in visual appearance and provide an idea of strath profile geometry. The plot for each valley was aligned so the anticlinal hinge (maximum strath separation) resides at a valley distance of 6 km. Incision downstream from a valley distance of ~9 km has been affected by recent anthropogenic incision (Appendix A). Bedrock cross sections constrained by surface bedding attitudes are shown in the lower half of each plot. Vertical exaggeration is 2.25X. Bedrock units are labeled as in Figure 2c, with the following additions: E, Epiligurian; Qst, Stirone Formation; Qcz, Costamezzana Formation; Qaf, Quaternary alluvium, undivided.

Table 2. Strath Dips and Average Rates of Dip Change[a]

	Taro		Parola		Stirone	
	Dip	Rate (°/Ma)	Dip	Rate (°/Ma)	Dip	Rate (°/Ma)
Valley	0.005		0.012		0.009	
Qt3	0.006	0.010	0.020	0.058		
Qt1	0.024	0.031			0.017	0.013
AES2			0.024	0.025		
AES1			0.038	0.040		

[a]Rates are calculated by subtracting the modern valley-bottom dip from the strath dip. Ages used for AES1 and AES2 rates are 825 and 775 ka, respectively.

younger than 1200 ka (beginning of middle Pleistocene) based on molluscan faunal assemblages [*Ciangherotti et al.*, 1997]. Southeast of the Salsomaggiore area along the range front, the Qt/Qa1 deposit is separated from AEI by the Imola Sands [*Amorosi et al.*, 1998b], which were not observed at Salsomaggiore. Rather, the AES1 and AES2 deposits separate AEI and Qt1. The age of the Imola Sands becomes younger toward the southeast, reflecting regression of the Adriatic Sea, and has an age of ∼800 ka constrained by paleomagnetic and electron spin resonance analyses near Forli [*Antoniazzi et al.*, 1993] and cosmogenic dating near Imola (D. Granger et al., unpublished data; see Figure 2b for locations). The thickness of the Imola Sands decreases northwest of Imola and pinches out somewhere between the Enza River (near Reggio Emilia, Figure 2b) and Salsomaggiore (G. Di Dio et al., personal communication, 2007). On the basis of these constraints, AES1 and AES2 have an age between ∼620–1200 ka, but probably closer to 800 ka, roughly correlative to the Imola Sands.

4.2. Strath Elevations: Terrace Profiles and Incision Rates

[29] Measured vertical separations between straths and modern valley bottoms are plotted above the Stirone, Parola, and Taro valley profiles in Figure 6. Notably, the Qt3 strath separation in the Taro valley (37 m) and Qt6 strath separation in the Stirone valley (10 m) are greatest at the valley location of the Salsomaggiore anticlinal hinge defined on the basis of the dips of Miocene bedrock (Figures 3 and 6). The location of the hinge is also coincident with a distinct convexity in the Parola valley profile (Figure 6b), as well as an abrupt bend in the Stirone valley (Figure 3). In addition, older strath profiles on the forelimb of the anticline have progressively steeper dips toward the Po foreland, the steepest strath dips occur near the Parola valley, and the average rate of change in strath dip has decreased near the Taro valley since Qt1 time (Figure 6 and Table 2).

[30] Maximum strath separations and associated incision rates are shown in Figure 7. Average incision rates are relatively constant in all valleys until Qt3 time (∼140 ka), since which the average incision rate has increased (Figure 7). The amount of incision that has taken place

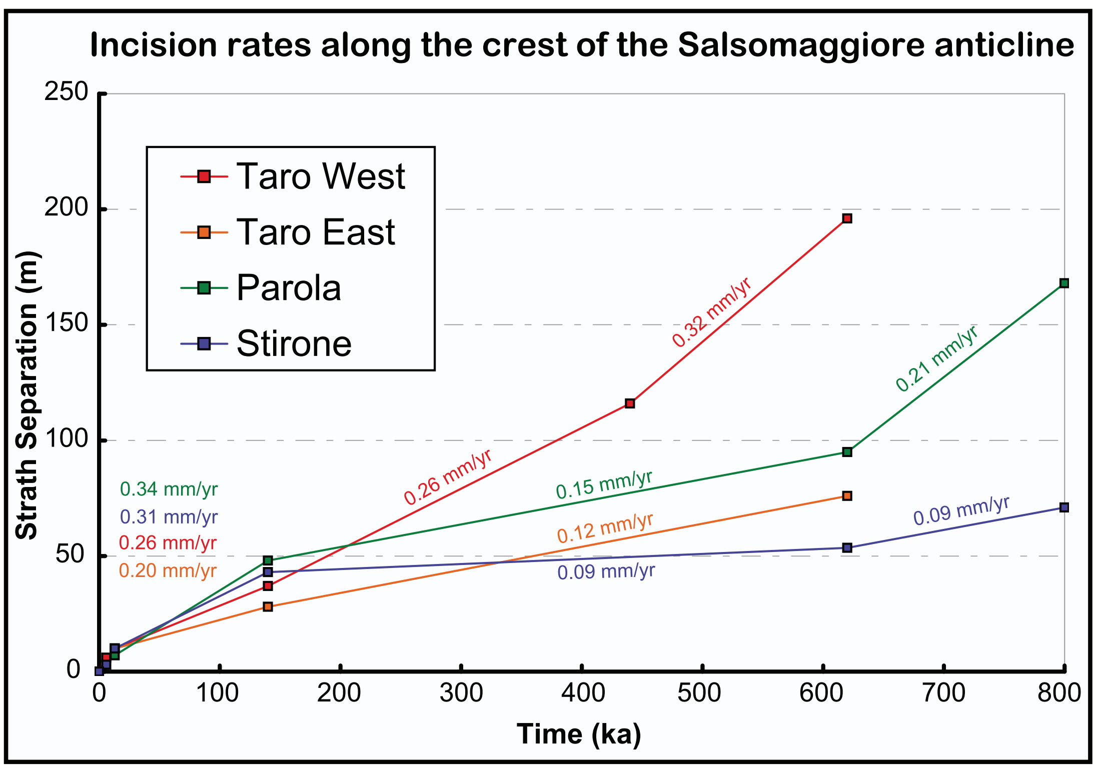

Figure 7. Graph showing inferred (projected) vertical separations between straths and modern valley bottoms at the crest (where incision is greatest) of the Salsomaggiore anticline in the Taro, Parola, and Stirone valleys. Since ∼620 ka (Qt1), the amount of incision that has taken place increases from the Stirone toward the west side of the Taro valley and decreases from the west to the east side of the Taro valley. In contrast, since ∼140 ka (Qt3), maximum incision has taken place in the Parola valley and gradually decreases toward the Stirone and Taro valleys.

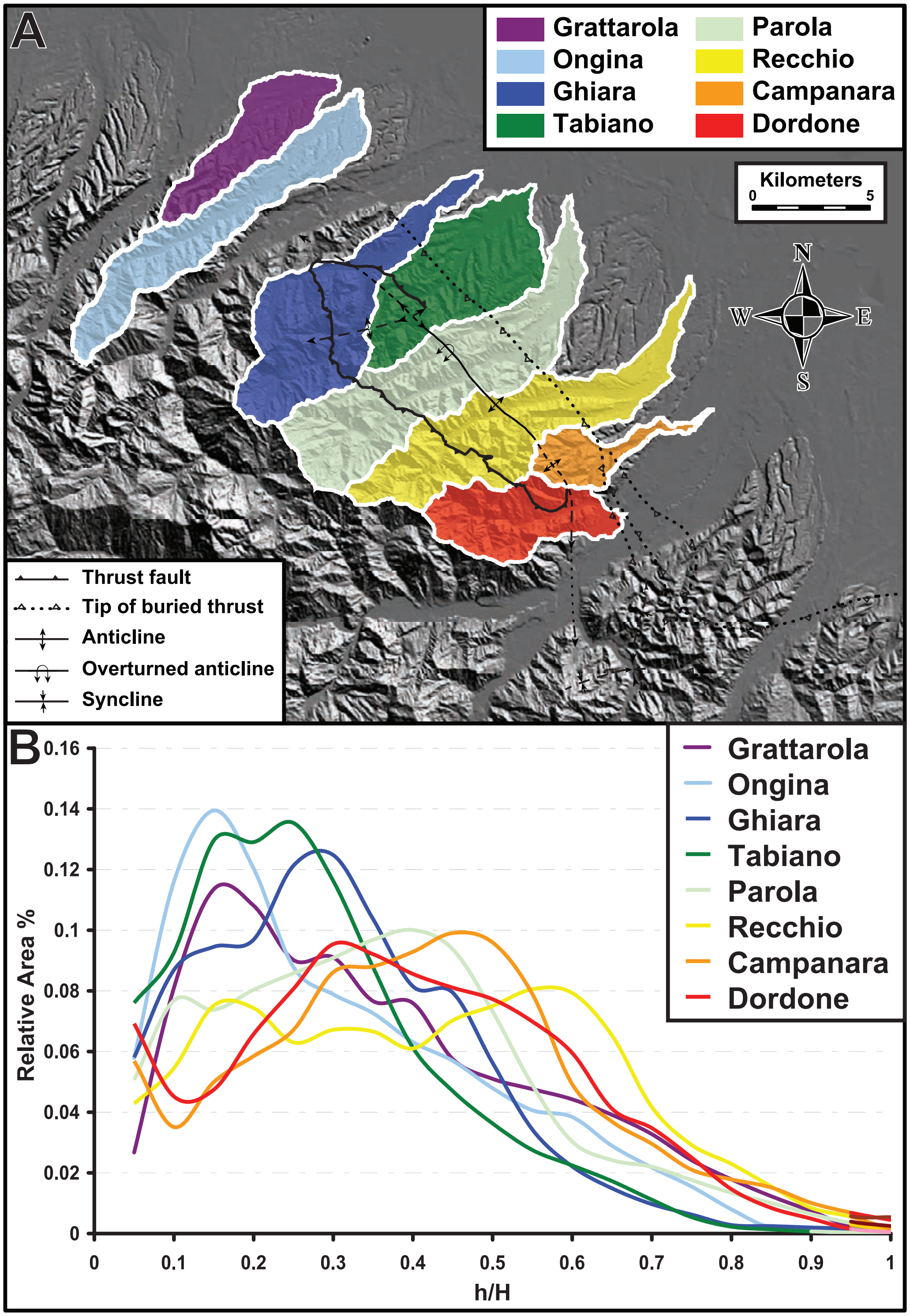

Figure 8. (a) DEM with outlines of catchments analyzed for hypsometry. The Stirone catchment was not analyzed because the upper half parallels the fold hinge, and therefore is not suitable for assessing along-strike variation. (b) Hypsometric curves of catchments outlined in Figure 8a. The general trend is that catchments represented by warmer colors, centered on the Recchio catchment, have higher relative percentages of their catchment areas at higher relative elevations.

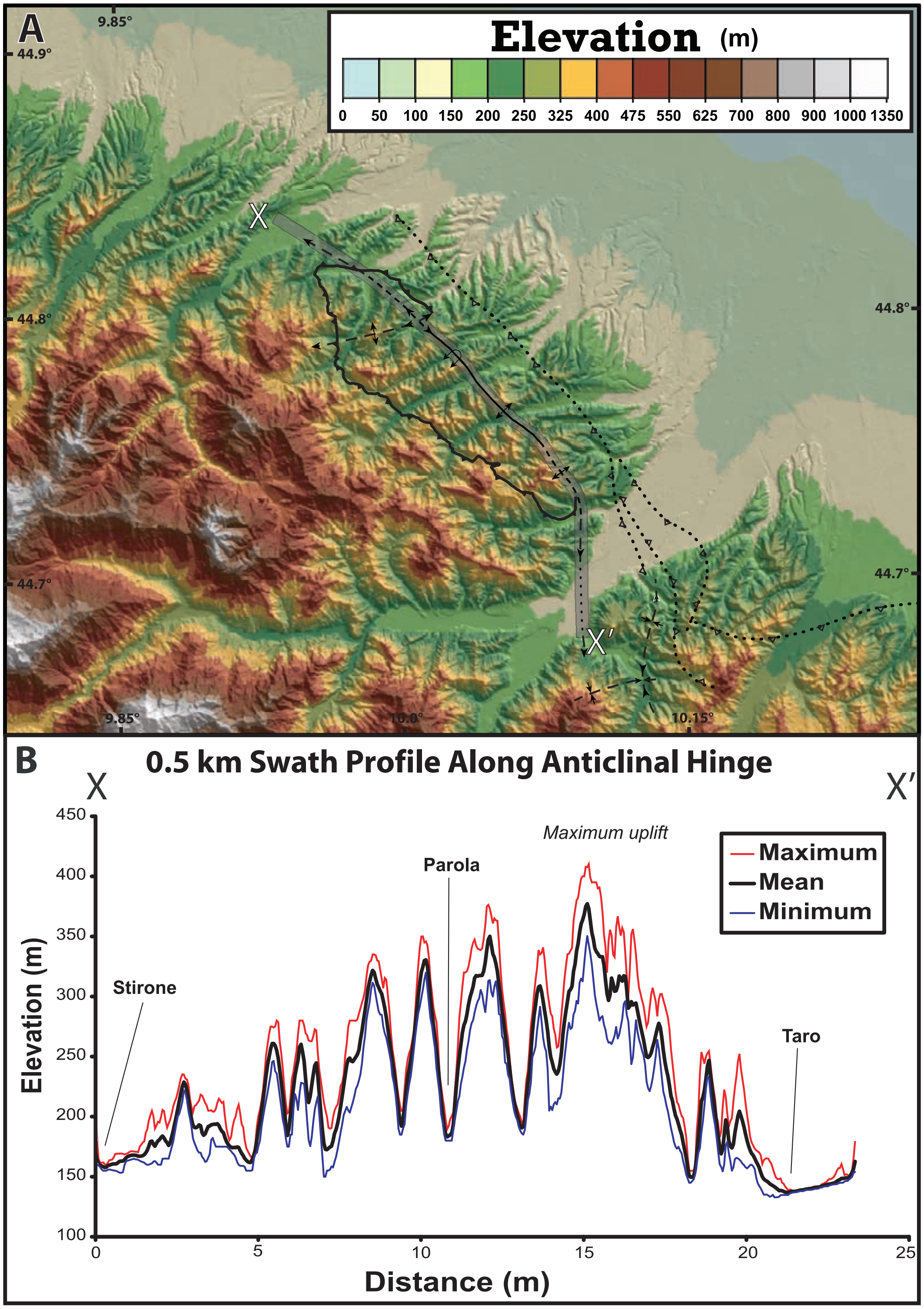

Figure 9. (a) 10 m DEM of the study area, colored to elevation and draped over a hill shade. (b) Swath topographic profile extracted from the DEM. The swath is 0.5 km wide, parallels the anticlinal hinge, and is delineated in Figure 9a.

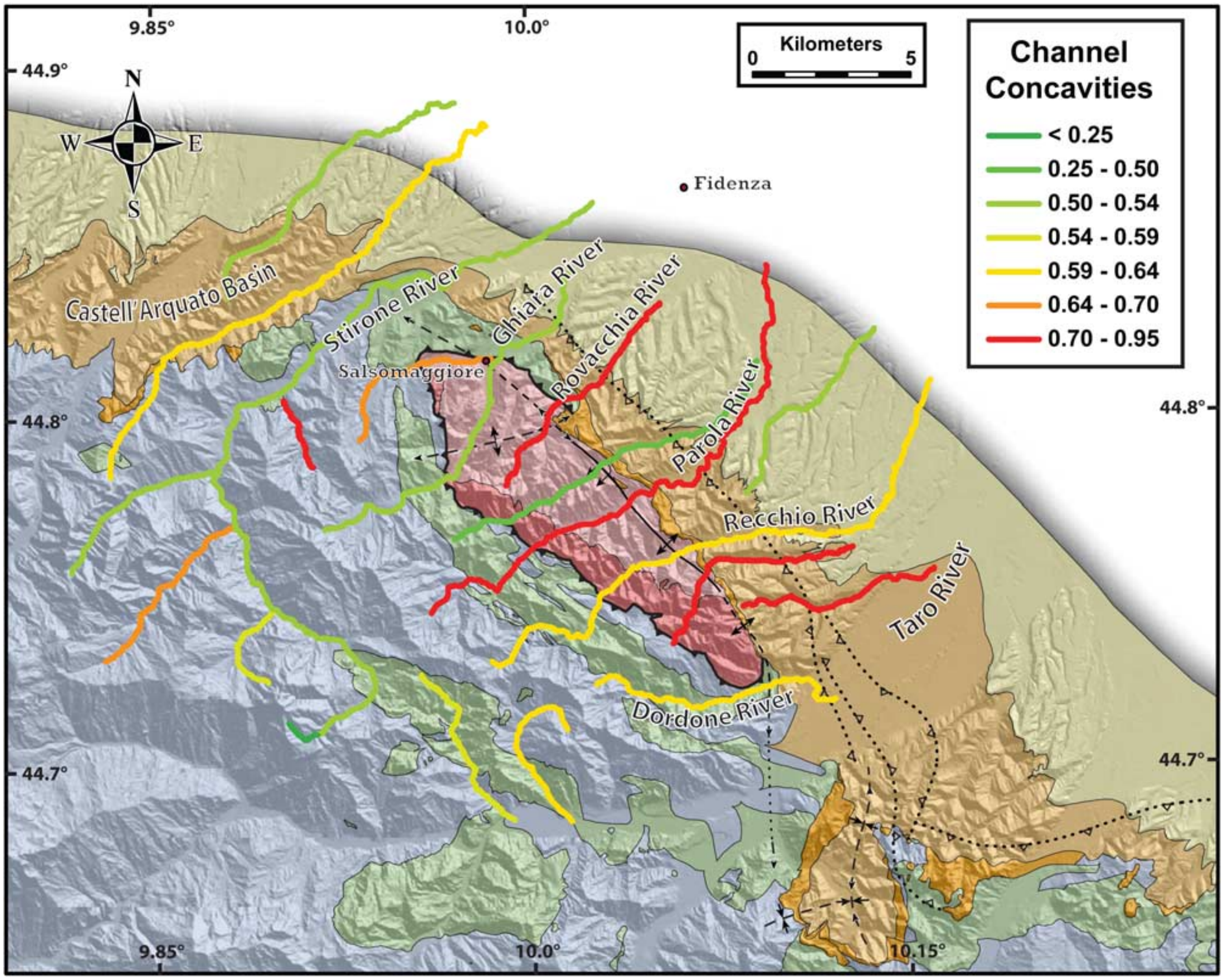

Figure 10. Channels are colored on the basis of concavity and draped over the bedrock geologic map. Channels that cross the forelimb at a high angle to the anticlinal hinge generally have higher concavity, and concavities generally increase from the Stirone toward the Taro valley.

since Qt1 time increases from the Stirone (54 m) toward the west side of the Taro valley (196 m), and decreases from the west to the east (76 m) side of the Taro valley. In contrast, since Qt3 time, the amount of incision that has taken place is greatest at the Parola valley (48 m) and gradually decreases toward the Stirone (43 m) and Taro valleys (37 m).

4.3. Topographic Metrics

[31] Variations in catchment hypsometries, mean anticlinal hinge elevation, and channel concavities mimic the gradual increase in the amount of middle Pleistocene-Recent incision from the Stirone eastward to the west side of the Taro River valley. Catchment hypsometries indicate a higher relative percent of land area at higher relative elevations in catchments approaching the Taro River from the northwest (Figure 8). Similarly, mean topographic elevation beneath the anticlinal hinge (Figure 9) and channel concavities (Figure 10) generally increase from the Stirone toward the Taro valley. Conversely, channel steepness indices correspond very closely with bedrock lithology, with higher k_{sn} calculated for channels underlain by easily erodable mudstones of the Ligurian and the Epiligurian deposits (Figure 11). Other notable reaches of locally high k_{sn} include the confluence of the Ghiara and Stirone channels in the lower Stirone valley, the confluence of the two main channels that make up the Ghiara catchment near the town of Salsomaggiore, and the intersection of channels with the coarse deposits of the Rio Gisolo Formation. Another peculiar observation noted in the field and visible on a DEM is the abundance of northwest transported earthflows and debris flows in the Parola and Gisolo catchments near the anticlinal hinge, as well as a 3 km across arcuate escarpment at this same location that serves as the drainage divide between the Parola and Recchio catchments (Figure 12).

5. Discussion

5.1. Fixed Anticlinal Hinge

[32] Fanning dips of Miocene-Pliocene strata on the forelimb of the anticline are consistent with an anticlinal hinge that was fixed in material during deposition. Folded

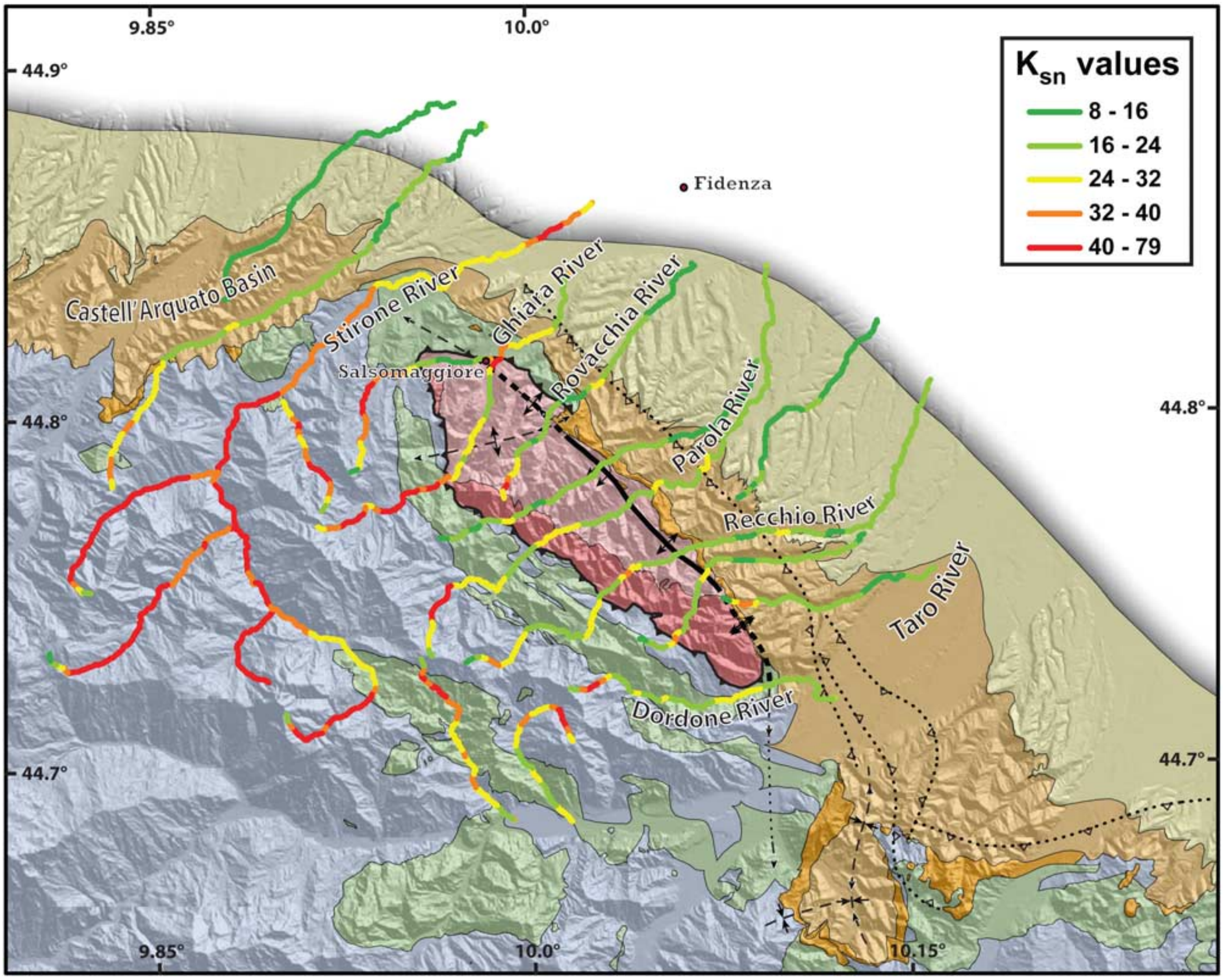

Figure 11. The k_{sn} values calculated for channel segments and color-coded to magnitude, draped over the bedrock geologic map. Note that increased k_{sn} coincide with the location of Ligurian (blue) and Epiligurian (green) deposits (legend for map units is shown in Figure 3).

strath profiles (Figure 6) confirm that incision has been driven by rock uplift associated with growth of the underlying anticline. Furthermore, the spatial coincidence of maximum strath separations (Figure 7), the Parola valley profile convexity, and an abrupt bend in the Stirone valley with the anticlinal hinge defined on the basis of the dips of Miocene bedrock (Figure 6) suggests the anticlinal hinge has remained fixed to material since Miocene time.

5.2. Rolling Synclinal Hinge

[33] Over long timescales representative of tectonic processes (>~100 ka), rivers incise uplifting rock and deposit their sediments in adjacent subsiding basins. During this time, straths and associated terrace deposits are gradually rotated about the zone that marks the transition from uplift to subsidence. If the zone that marks the boundary between regions of uplift and subsidence does not migrate laterally through time, uplifted terrace deposits will intersect (or project to) the modern valley profile at a fixed location [e.g., *Picotti and Pazzaglia*, 2008]. If, however, the boundary between regions of uplift and subsidence shifts laterally over these relatively long timescales, alluvial deposits near the range front will subside or be uplifted accordingly. If the zone that separates regions of uplift and subsidence migrates in the direction of the region of subsidence, old intersection points will be uplifted above the valley profile, and the point at which those older alluvial deposits intersect the modern valley profile today will have migrated in the direction of the region of subsidence. This is precisely the case at Salsomaggiore.

[34] On the west side of the Taro valley, just downstream from the town of Medesano, the Qt3 deposit overlies Qa1 gravels that project updip into the Qt1 terrace, which is exposed above Medesano (Figures 4 and 13a). At this location above Medesano, the Qt3 terrace is inset into and topographically lower than Qt1, which requires that the Qt1 and Qt3 terrace deposits intersect between the exposures displayed in Figure 13a. The implication is that the transition from uplifting anticline to subsiding basin since Qt3 time has migrated toward the foreland, causing uplift of alluvial deposits (Qa1) that formerly subsided below the

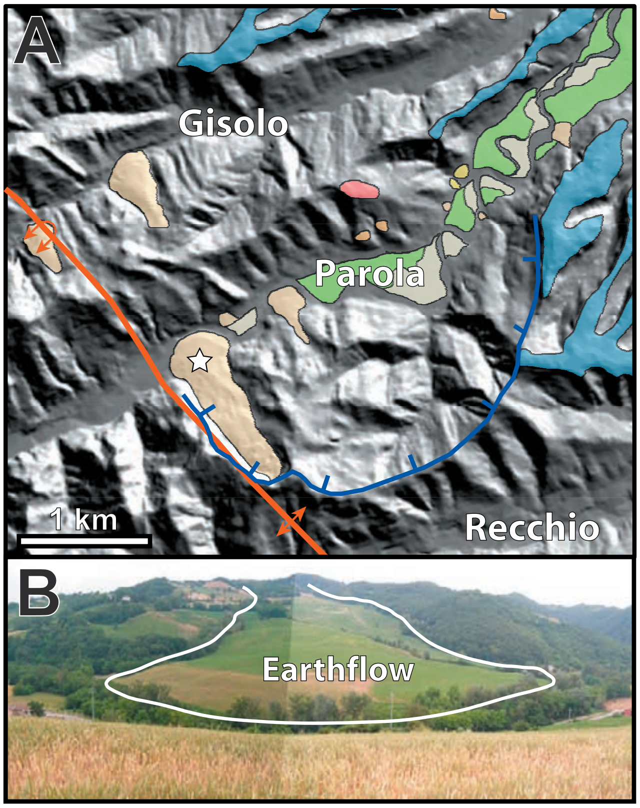

Figure 12. (a) Mapped surficial deposits and terraces as shown in Figure 4 draped over DEM hill shade. Legend and outline of area is shown in Figure 4. Note the abundant northwest transported earthflows and debris flows and the large arcuate escarpment that serves as the Parola-Recchio drainage divide. (b) A recent, large earthflow in the Parola valley. A star is placed over this deposit in Figure 12a to reference location and scale.

level of the modern valley profile (and were covered by deposition of Qt3 alluvium). The same relationship between Qt1 and Qt3 is clearly shown in map view on the west side of the Stirone valley (Figures 4 and 13b). These relationships suggest the presence of a rolling synclinal hinge over the past ~140 ka. As the synclinal hinge rolls forward, deposits that previously subsided below the level of the modern valley profile are incorporated into the lengthening forelimb and uplifted above the modern valley profile.

5.3. Fold Amplification Processes

[35] Fault-related folds have been described to amplify by two fundamental, end-member processes: limb rotation and limb lengthening (Figure 14). Limb rotation is characterized by a progressive limb spin without lengthening and predicts growth strata (strath profiles) with variable thickness and dip [e.g., *Riba*, 1976; *Hardy and Poblet*, 1994; *Ford et al.*, 1997]. Limb lengthening (a.k.a. hinge migration) is characterized by migration of material through axial surfaces, which are relatively narrow zones that separate beds of different dip [*Suppe*, 1983; *Suppe and Medwedeff*, 1990]. In contrast to limb rotation, hinge migration predicts fold limbs and growth strata (strath profiles) with constant dip. However, *Suppe et al.* [1997] showed that gradual rather than abrupt curvature of beds across axial surfaces results in fanning growth strata dips on fold limbs at shallow depths, even during pure limb lengthening. Any number of kinematic scenarios is possible that incorporate solely limb rotation, limb lengthening, or some combination of the two over part or all of a fault-related fold's growth history. The predictions of these fold amplification mechanisms are testable and have been constrained in other regions using fluvial terrace geometry [*Scharer et al.*, 2006].

[36] The fanning dips of Miocene-Pliocene strata on the forelimb of the Salsomaggiore anticline are consistent with growth dominated by limb rotation about a fixed anticlinal hinge. In contrast, the recent uplift of intersected fluvial deposits documents forelimb lengthening by synclinal hinge migration, possibly suggesting a Pleistocene shift in shortening mechanism. Fanning strath profile dips (Figure 6) may reflect limb rotation in combination with limb lengthening, but are also explained by curved-hinge migration [*Suppe et al.*, 1997; *Scharer et al.*, 2006], an alternative supported by strath dips of less than 1 degree (Table 2), compared to Pliocene bedding dips of 10–45 degrees. A change in the mechanism of growth of the Salsomaggiore anticline from limb rotation to limb lengthening would not be surprising because strain hardening occurs as flexural folds tighten and the bedding anisotropy is progressively rotated to a high angle to the principle shortening direction [e.g., *Woodward*, 1997]; it is more energetically favorable to lengthen the forelimb than to continue to rotate the forelimb after the dip becomes exceptionally steep. This interpretation is also consistent with the cross sections of *Picotti et al.* [2007] that suggest relatively recent formation of two break-back imbricates above the main Salsomaggiore thrust; creation of new imbricates is another alternative to continued limb rotation to accommodate shortening.

5.4. Fault Tip Propagation

[37] In numerous well-constrained natural examples of fault-propagation folding, the synclinal axial surface of a fault-propagation fold is tied at depth to the fault tip [e.g., *Suppe and Medwedeff*, 1990]. Therefore, if the vertical and lateral translation of the Qt/Qa1 intersection point since Qt3 time serves as an estimate of the amount of synclinal hinge migration, it may serve as a proxy for propagation of the fault tip (Figure 15), a process that is rarely constrained with data [*Allmendinger and Shaw*, 2000; *Jackson et al.*, 2002]. Across the Salsomaggiore anticline, some of the forward migration of the Qt1 intersection point since Qt3 time reflects recent anthropogenic incision (Appendix A). In the Parola and Stirone valleys, the increase in incision rates between Qt3 and Qt6 time (Figure 7) has also affected where the Qt1 deposit intersects the modern valley profile. If this increase in incision rates reflects the unsteady nature of fluvial incision in response to climate change [e.g., *Hancock and Anderson*, 2002] (rather than an increase in rock uplift rates), it can be corrected for by artificially lowering the valley profile from the Qt3 strath at the long-term incision rate. In the Taro valley, incision up until the late Pleistocene occurred at a fairly steady rate, so solely removing recent anthropogenic incision allows for an accurate estimate of the long-term rate of forward migration of the Qt1 intersection point. Accounting for 5 m of anthropogenic incision (Appendix A) and using strath elevations from the west side of the Taro valley suggests the fault tip

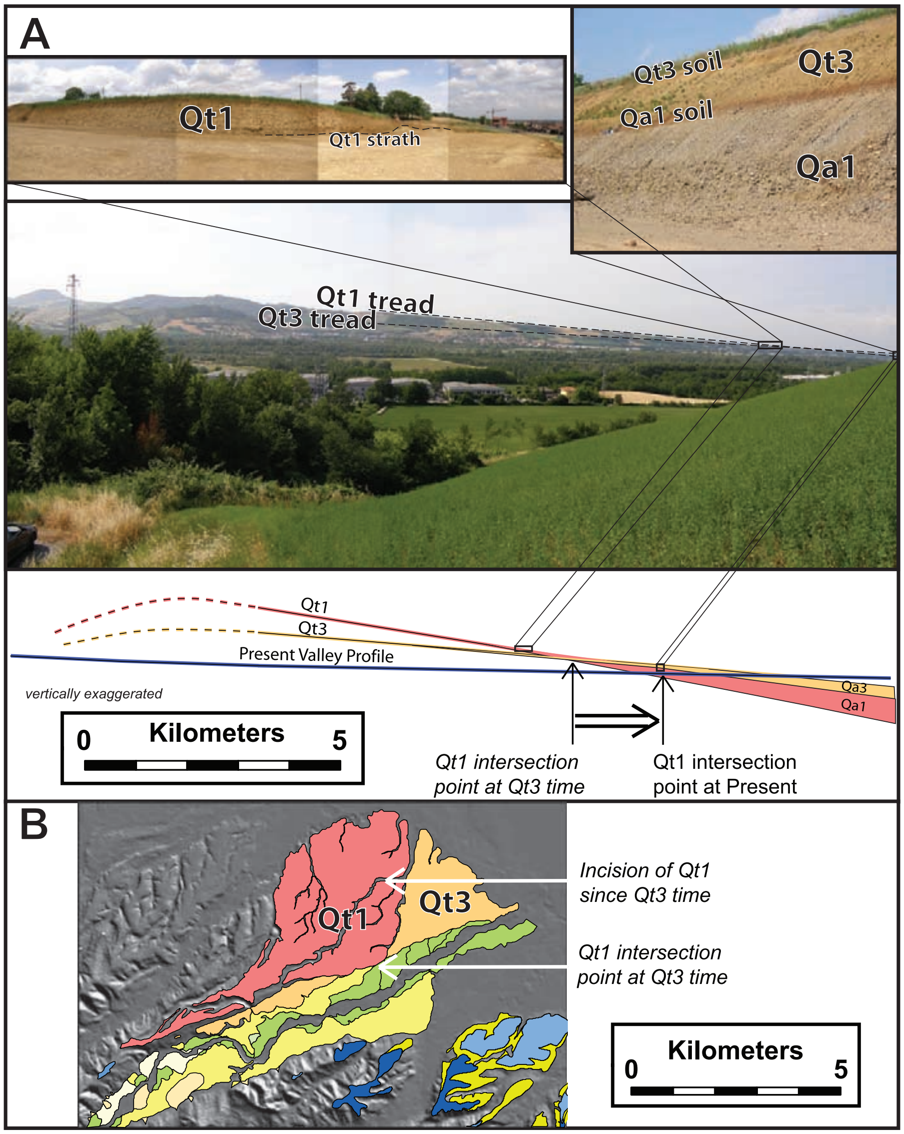

Figure 13. (a) Intersection points in cross-section view demonstrated by outcrops on the west side of the Taro valley. Upstream from the intersection point, Qt3 is inset into Qt1, while downstream Qt3 was deposited on top of the Qa1 (time-correlative to Qt1 strath) deposit. (b) The same Qt3-Qt1 intersection shown in map view in the Stirone valley; legend for units is shown in Figure 4.

has propagated ~2 km forward at an average rate of 1.4 cm/a over the past 140 ka. This also implies the limb has lengthened by 2 km over the same time. Examination of the location of the Qt3-Qt1 intersection points in map view reveals the intersection point at the strike of the west side of the Taro valley is located farther (~6.0 km) from the anticlinal hinge than the intersection point in the Stirone valley (~4.5 km). This suggests more limb lengthening and more fault tip propagation has occurred at the strike of the Taro valley than the Stirone valley.

5.5. Along-Strike Variations in Uplift and Forelimb Tilting

[38] The gradual increase in pre-Qt3 strath separation (Figure 7), catchment hypsometries with a greater proportion of higher relative elevations (Figure 8), and mean anticlinal hinge elevation (Figure 9) from the Stirone toward the Taro valley point to an along-strike gradient in middle Pleistocene-Recent uplift. An along-strike maximum in uplift near the east side of the Recchio valley and west side of the Taro valley is suggested by catchment hypsometry, maximum anticlinal hinge elevations, and the abundant northwest transported mass wasting deposits (Figure 12) on the northwest flank of this area. The mass wasting features may be partly related to north aspect slopes, but such features are not observed elsewhere in the study area. Probably, this along-strike uplift gradient reflects an increase in the amount of fault propagation and limb lengthening at the strike of the Taro valley. Additionally, it may reflect curvature of the Salsomaggiore thrust (Figure 3);

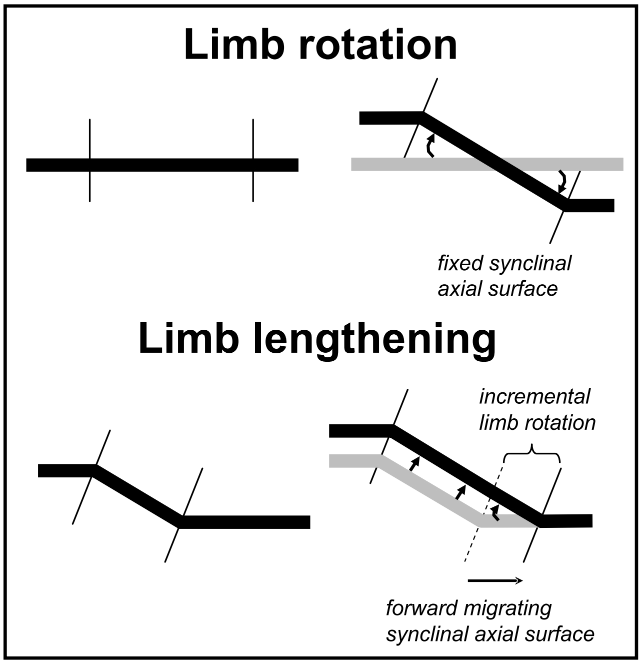

Figure 14. Schematic illustration of the two end-member mechanisms by which folds amplify to accommodate shortening. (top) Limb rotation results in growth strath and strath profiles with constant limb length and variable limb dip, and the limb is bound by rotating axial surfaces. (bottom) Limb lengthening results in self-similar growth: growth strata and strata profile dips remain constant as the limb lengthens, and the axial surfaces do not rotate.

steepening of the Salsomaggiore thrust, though precise ramp dip is unknown; an increase in the amount of dip slip associated with the change in trend of the Salsomaggiore thrust; and/or focusing of deformation by the Taro River [*Simpson*, 2004].

[39] Greater Qt3 strath separation at the strike of the Parola valley than the Stirone or Taro valleys (Figure 7) could mean that the fulcrum of uplift associated with growth of the underlying fold has migrated from the west side of the Taro valley to the Parola valley since Qt3 time. Alternatively, this may reflect that smaller, steeper channels undergoing the same adjustments in concavity as larger channels should experience greater incision along the reaches of the channels analyzed in this study. The lower, gently dipping reach of the Taro River will not change in vertical position as much as the Parola channel given the same adjustments in channel concavity. This alternative explanation predicts maximum incision by the smallest rivers, consistent with the decrease in the amount of incision since Qt3 time in order of the Parola, Stirone, and Taro channels.

[40] Although adjustments in channel concavity may be partly responsible for along-strike differences in channel incision since Qt3 time, channel concavity adjustments cannot be responsible for all incision extending back to ~800 ka. As a sensitivity test, synthetic channel profiles were generated with variable concavity, equal in total relief and length to the modern Parola channel (Figure B1). An increase in concavity from 0.5 to 0.75 (the modern Parola concavity) results in a few 10s and a maximum of 100 m of incision, most of which takes place in the upper half of the catchment where the slope is steeper. The channel in the lower half of the catchment experiences less than 50 m of incision. In contrast, the AES1 deposit resides 107 m above the modern channel in the lower half of the Parola catchment and 168 m above the modern channel when projected up dip to the anticlinal hinge. The effect of adjustments of channel concavity on incision is particularly reduced in the Taro valley compared to the Parola valley, yet Qt1 deposits reside 196 m above the Taro channel when projected up dip to the anticlinal hinge. These observations suggest the record of incision since Qt3 time reflects both rock uplift and channel concavity adjustments, but the net incision since pre-Qt3 time mainly reflects rock uplift associated with growth of the underlying fold. Because the average incision rate has remained relatively constant throughout the span of the terrace record in the Taro valley, Taro channel concavity adjustments across the reach that intersects the study area have likely been minimal and not affected the calculation of the rate of synclinal hinge migration and limb lengthening. These results underscore the utility of using large drainages like the Taro (rather than the Parola) that are at or near their base level of erosion in drawing conclusions about tectonic activity from incision data.

[41] The location of maximum forelimb rotation rate has varied during growth of the Salsomaggiore anticline. A steeper modern Parola valley profile does not explain the steeper strath profiles at that location (Figure 6 and Table 2), because the oldest (AES1 and AES2) terrace deposits preserved above the Parola channel were deposited by the lower gradient, paleo-Taro River. Discounting a long-term shallowing of the Taro valley profile gradient, straths above the Parola valley must reflect a middle Pleistocene to Recent peak in forelimb rotation that does not coincide with the location of maximum uplift, requiring greatest horizontal rock advection at the strike of the Parola valley. If true, this indicates the location of maximum forelimb rotation rate has oscillated between the Taro and Parola valleys since the Miocene, because Pliocene strata (Argille Lugagnano) are most steeply dipping near the west side of the Taro valley and Miocene strata are most steeply dipping at the strike of the Parola valley [*Di Dio et al.*, 2005].

5.6. Fault Slip and P/S Ratios

[42] A nearly linear relationship between fault slip rate and crestal uplift rate is predicted for single-step, flexural-slip, fault-propagation folds with ramp dips greater than ~40 degrees and uplift rates less than ~1 mm/a [*Hardy and Poblet*, 2005]. Therefore, variations in long-term averaged incision at the crest of the Salsomaggiore anticline are directly comparable to variations in slip rate. Crestal incision and fault slip rates have been nearly constant throughout the span of the terrace record, with the possible exception of an increase since Qt3 time at the strike of the Parola and Stirone valleys. We are not able to calculate absolute fault slip rates because that requires knowledge of strath uplift relative to the footwall [e.g., *Lavé and Avouac*, 2000; *Picotti and Pazzaglia*, 2008; *Wegmann and Pazzaglia*, 2009], while we referenced straths to modern valley bottoms. Assuming an average sedimentation rate compa-

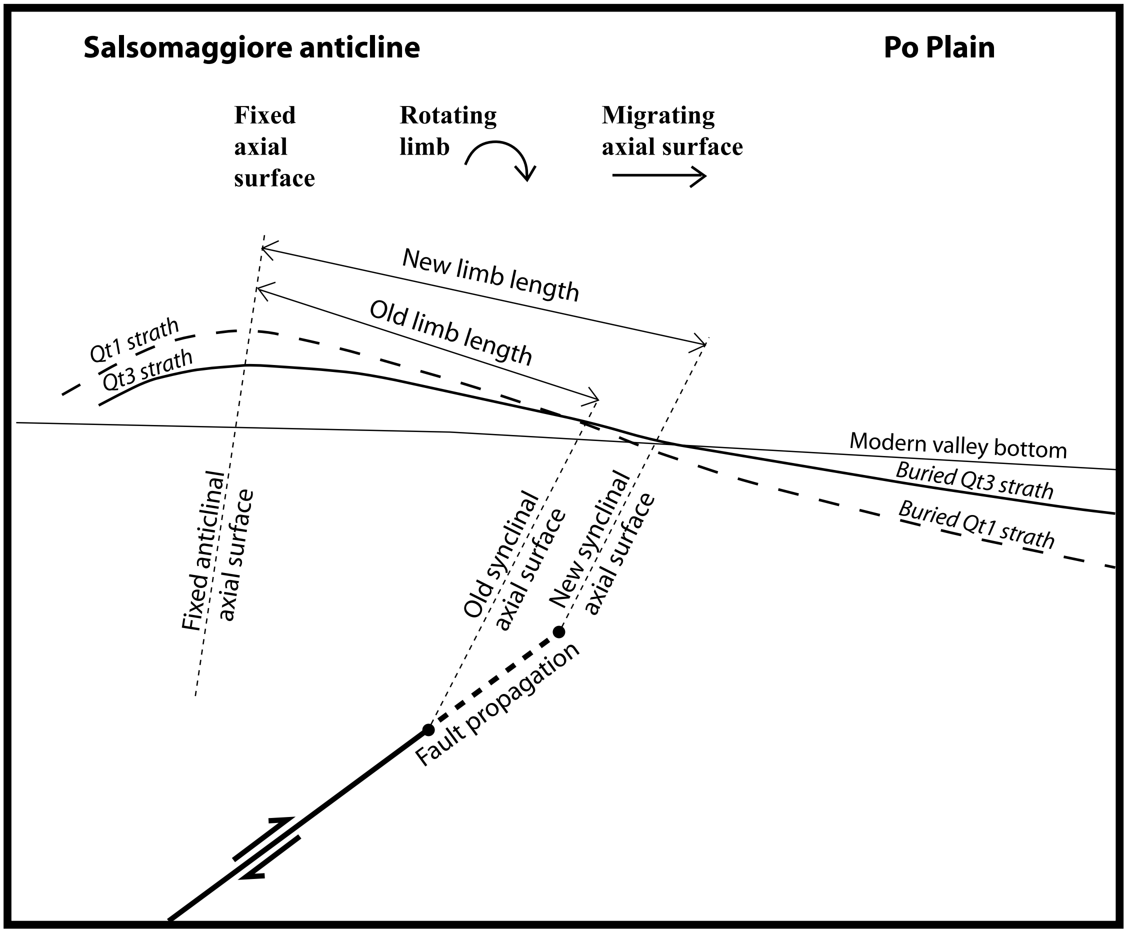

Figure 15. Schematic cross section of a fault-propagation fold illustrating the key constraints on fault propagation and fold kinematics proposed in this study. Forward migration of the synclinal axial surface reflects propagation of the fault tip.

rable to crestal incision rates (0.1–0.3 mm/a), crestal uplift rates relative to the footwall are 0.2–0.6 mm/a and fault slip rates should be less than ~0.5 mm/a. The decrease in strath rotation rate along the west side of the Taro valley since Qt1 time (Table 2), coupled with the near steady state uplift (incision) and fault slip rates, may argue for an increasing proportion of fold amplification accommodated by limb lengthening/hinge migration and a decreasing proportion accommodated by limb rotation. This interpretation would imply faster synclinal axial surface migration and fault tip propagation rates, as well as an increased propagation-to-slip ratio since Qt3 time. A fault tip propagation rate of 1.4 cm/a implies the propagation to slip ratio (P/S) is greater than ~3 near the Taro valley; if maintained, the Salsomaggiore thrust should become emergent within the next ~200 ka. (Figure 2c).

5.7. Channel Concavities and Steepness Indices

[43] The close correlation between channel k_{sn} and lithology (Figure 11) above a fold that is clearly growing suggests there may be a restricted range of rock uplift rates that strongly influence channel k_{sn}, and that the rock uplift rates that led to the measured incision rates (0.1–0.3 mm/a) are below that range. The somewhat inverse relationship between concavities (Figure 10) and k_{sn} is expected because these metrics are naturally autocorrelated. However, the coincidence of channels that cross the forelimb at a high angle to the fold hinge and generally higher concavities may partly reflect uplift and lateral advection of rock associated with growth of the anticline. *Kirby and Whipple* [2001] showed that when considering an equilibrium channel profile and a simple uplift equation that yields a power law gradient-area relationship, decreased uplift rates in the downstream direction should result in higher channel concavities. Similar to results of this study, *Kirby and Whipple* [2001] found that channels transverse and on the flank of an actively growing fold had higher concavities than channels that paralleled the fold hinge. This explanation is consistent with the general increase in channel concavities from the Stirone toward the Taro valley, mimicking along-strike variations in uplift; where there is greater uplift (near the Taro valley) there is a greater downstream decrease in uplift rates.

6. Conclusion

[44] The age and geometry of fluvial terrace deposits preserved across the forelimb and in river valleys dissecting

the Salsomaggiore anticline constrains the Pleistocene-Recent kinematics of the underlying fault-propagation fold. Strath profiles and map patterns document a fixed anticlinal hinge, a rolling synclinal hinge, and along-strike variations in uplift and forelimb tilting. Recognition of the uplifted intersection of alluvial deposits of different age, coupled with the fixed anticlinal hinge, allows inference of limb lengthening via synclinal hinge migration, and may serve as a marker of the amount of underlying fault tip propagation. Channel steepness indices are adjusted to bedrock lithology, not uplift, while channel concavities are higher on the forelimb, possibly owing to the downstream decrease in rock uplift rate. Along-strike variation in catchment hypsometries and the mean elevation of the anticlinal hinge mimic the incision/uplift recorded by fluvial terraces, and major landsliding is occurring near the location of maximum uplift. In contrast to recent growth dominated by limb lengthening, a synthesis of the Miocene-early Pleistocene history reveals fold growth with significant limb rotation, and complicated by fault-bend folding above a deeper lateral ramp. This study offers new insight into the recent and ancient growth of Salsomaggiore anticline and provides a novel demonstration of how fluvial terraces may be utilized to constrain fault-related fold kinematics.

Appendix A: Anthropogenic Incision

[45] In the early 1950s, gravel was extracted from the Stirone channel near the town of Fidenza for roads and buildings. Immediately following, a knickpoint was generated that rapidly propagated upstream: an incision response triggered by removal of channel armor and/or disruption of the slope-load-discharge balance. The knickpoint in the Stirone channel propagated upstream ~7 km and is now stabilized by concrete below a bridge at the town of Scipione Ponte [*Brugnara and Zannoner*, 1997]. Upstream from the bridge, Qt9 is nonexistent and essentially coincides with the modern valley bottom. Downstream from the bridge, Qt9 is separated from the modern stream channel by as much as 5 m, creating spectacular exposures of the

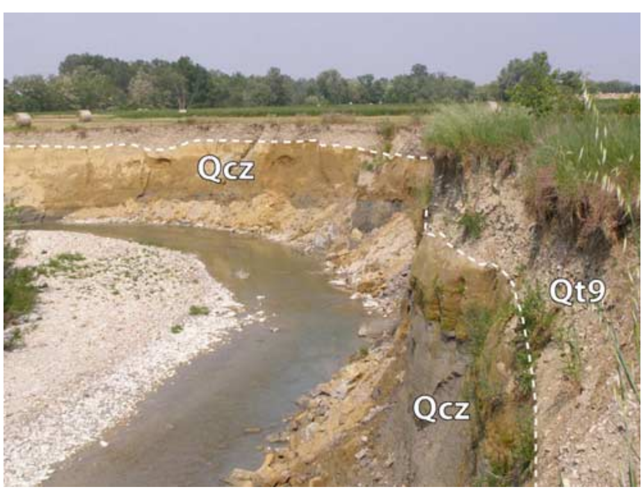

Figure A1. Photograph of recently exposed, gently dipping Costamezzana Formation (Qcz) capped by Qt9 terrace above the Stirone channel.

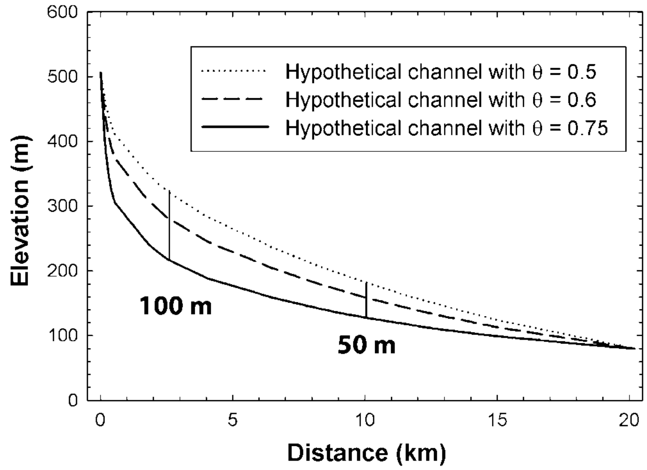

Figure B1. Parola channel concavity calculations. Vertically exaggerated. A maximum of 100 m of incision occurs with a change in concavity from 0.5 to 0.75 and less than 50 m occurs in the lower half of the catchment.

Pliocene-Pleistocene bedrock (Figure A1), which have served as a framework for a plethora of stratigraphic studies over the past few decades. Because of this phenomenon in the Stirone valley, terrace straths (especially Qt6) should be considered relative to the Qt9 strath at valley locations downstream from Scipione Ponte. Similar knickpoints associated with recent anthropogenic incision are visible on Ghiara, Rovacchia, and Recchio stream longitudinal profiles created from a 10 m digital elevation model, as well as the Taro valley longitudinal profile (Figure 6). A knickpoint is not visible on the Parola longitudinal profile: either a knickpoint was not created in this channel or the channel has accommodated the incision by increasing its sinuosity instead. The latter possibility is consistent with the anomalously high sinuosity of the Parola channel relative to the adjacent channels, visible in Figure 3. However, part of this sinuosity is a result of recent debris flows and earthflows that have "pushed" the channel to the opposite side of the valley (Figure 12).

Appendix B: Channel Concavity Adjustments

[46] Figure B1 shows synthetic channel profiles of variable concavity, equal in total relief and length to the modern Parola channel. The head of the channel is defined at the inflection on a plot of slope and upstream drainage area in log-log space. Synthetic channels were calculated utilizing the slope-area and distance-area relationships of the modern Parola channel. Holding k_s and area constant, incremental channel length and slope were calculated for θ of 0.5, 0.6, and 0.75.

[47] **Acknowledgments.** This paper is based on the Master's thesis of L. Wilson, completed at Lehigh University in 2008. Research was funded by a grant from the Palmer fund of the Department of Earth and Environmental Sciences at Lehigh University, stipend and tuition support from a Kravis Fellowship and a College of Arts and Sciences Teaching Assistantship, the Arthur A. Meyeroff Memorial Grant from the American Association of Petroleum Geologists Grants-In-Aid program, a student research grant from the Geological Society of America, and a National Science Foundation Continental Dynamics Grant (F. J. Pazzaglia, P.I., EAR-0207980 RETREAT). We kindly thank J. P. Avouac and an anony-

mous person for thoughtful reviews that improved the manuscript; V. Picotti for suggesting the study location, introducing us to the field area, and providing insight into the local geology; J. Wilson for support and help with field work; A. Ponza for help coordinating field work and obtaining digital data; the Regione Emilia Romanga geologic survey for digital data; A. Artoni, G. Papani, and G. Di Dio for their help obtaining data and their discussions on the geology at Salsomaggiore; G. Santos and the Keck-CCAMS group at the University of California Irvine for performing the radiocarbon analyses; S. Bruna for her hospitality and accommodations at Casa Bruna; and ExxonMobil for funding publication of the manuscript.

References

Ahmadi, R., J. Ouali, E. Mercier, J. L. Mansy, B. V. V. Lanoë, P. Launeau, F. Rhekhiss, and S. Rafini (2006), The geomorphologic responses to hinge migration in the fault-related folds in the southern Tunisian Atlas, *J. Struct. Geol.*, *28*, 721–728, doi:10.1016/j.jsg.2006.01.004.

Allmendinger, R. W. (1998), Inverse and forward numerical modeling of trishear fault-propagation folds, *Tectonics*, *17*, 640–656, doi:10.1029/98TC01907.

Allmendinger, R. W., and J. H. Shaw (2000), Estimation of fault propagation distance from fold shape: Implications for earthquake hazard assessment, *Geology*, *28*, 1099–1102, doi:10.1130/0091-7613(2000)28<1099:EOFPDF>2.0.CO;2.

Amorosi, A., M. Farina, P. Severi, D. Preti, L. Caporale, and G. Di Dio (1996), Genetically related alluvial deposits across active fault zones: An example of alluvial fan-terrace correlation from the upper Quaternary of the southern Po Basin, Italy, *Sediment. Geol.*, *102*, 275–295.

Amorosi, A., M. Barbieri, F. Castorina, M. L. Colalongo, G. Pasini, and S. C. Vaiani (1998a), Sedimentology, micropaleontology, and strontium-isotope dating of a lower-middle Pleistocene marine succession (Argille Azzurre) in the Romagna Apennines, northern Italy, *Boll. Soc. Geol. Ital.*, *117*(3), 789–806.

Amorosi, A., L. Caporale, U. Cibin, M. L. Colalongo, G. Pasini, F. Ricci Lucchi, P. Severi, and S. C. Vaiani (1998b), The Pleistocene littoral deposits (Imola Sands) of the northern Apennines foothills, *G. Geol.*, *60*(3A), 83–118.

Amorosi, A., L. Forlani, F. Fusco, and P. Severi (2002), Cyclic patterns of facies and pollen associations from late Quaternary deposits in the subsurface of Bologna, *GeoActa*, *1*, 83–94.

Anastasio, D. J., D. M. Fisher, T. A. Messina, and J. E. Holl (1997), Kinematics of décollement folding in the Lost River Range, Idaho, *J. Struct. Geol.*, *19*, 355–368, doi:10.1016/S0191-8141(97)83028-3.

Antoniazzi, A., M. Ferrari, and C. Peretto (1993), Il giacimento di Ca' Belvedere di Monte Poggiolo del Pleistocene inferiore con industria litica (Forlì), *Boll. Soc. Paleontol. Ital.*, *84*, 1–56.

Artoni, A. (2003), La sezione stratigrafica del T. Parola (Salsomaggiore, Parma; Appennino Emiliano): Confronto con le successioni ipoaline messiniane del margine appenninico padano, *Acta Nat. de L'Ateneo Parmense*, *39*, 5–30.

Artoni, A., G. Papani, F. Rizzini, M. Calderoni, M. Bernini, A. Argnani, M. Roveri, M. Rossi, S. Rogledi, and R. Gennari (2004), The Salsomaggiore structure (northwestern Apennine foothills, Italy): A Messinian mountain front shaped by mass-wasting products, *GeoActa*, *3*, 107–127.

Artoni, A., F. Rizzini, M. Roveri, R. Gennari, V. Manzi, G. Papani, and M. Bernini (2007), Tectonic and climatic controls on sedimentation in the late Miocene Cortemaggiroe wedge-top basin (northwestern Apennines), in *Thrust Belts and Foreland Basins, From Fold Kinematics to Hydrocarbon Systems*, edited by O. Lacombe et al., pp. 431–456, Springer, Berlin.

Benedetti, L., P. Tapponnier, G. C. P. King, B. Meyer, and I. Manighetti (2000), Growth folding and active thrusting in the Montello region, northern Italy, *J. Geophys. Res.*, *105*(B1), 739–766, doi:10.1029/1999JB900222.

Bernard, S., J.-P. Avouac, S. Dominguez, and M. Simoes (2007), Kinematics of fault-related folding derived from a sandbox experiment, *J. Geophys. Res.*, *112*, B03S12, doi:10.1029/2005JB004149.

Bigi, G., D. Consentino, M. Parotto, R. Sartori, and P. Scandone (1990), Structural model of Italy, scale 1:500,000, Società Elaborazioni Cartografiche, Consiglio Nazionale della Ricerche Progetto Finalizzato Geodinamica, Firenze, Italy.

Brugnara, R., and C. Zannoner (1997), *Parco Regionale Fluviale dello Stirone*, 197 pp., Giunti, Firenze, Italy.

Bull, W. B. (1991), *Geomorphic Response to Climatic Change*, 326 pp., Oxford Univ. Press, New York.

Casas-Sainz, A. M., R. Soto-Marín, Á. González, and J. J. Villalaín (2005), Folded onlap geometries: Implications for recognition of syn-sedimentary folds, *J. Struct. Geol.*, *27*, 1644–1657, doi:10.1016/j.jsg.2005.05.005.

Castellarin, A., and G. B. Vai (1986), Southalpine versus Po Plain Apenninic arcs, in *The Origin of Arcs: Developments in Geotectonics*, edited by F. C. Wezel, pp. 253–280, Elsevier, Amsterdam.

Channell, J. E. T., M. S. Poli, D. Rio, R. Sprovieri, and G. Villa (1994), Magnetic stratigraphy and biostratigraphy of Pliocene "argille azure" (northern Apennines, Italy), *Palaeogeogr. Palaeoclimatol. Palaeoecol.*, *110*, 83–102, doi:10.1016/0031-0182(94)90111-2.

Ciangherotti, A. D., P. Crispino, and D. Esu (1997), Paleoecology of the non-marine molluscs of the Pleistocene Stirone River sequence (Emilia, Northern Italy), *Boll. Soc. Paleontol. Ital.*, *36*, 303–310.

Conti, S., A. Artoni, and G. Piola (2007), Seep-carbonates in a thrust-related anticline at the leading edge of an orogenic wedge: The case of the middle-late Miocene Salsomaggiore ridge (northern Apennines, Italy), *Sediment. Geol.*, *199*, 233–251, doi:10.1016/j.sedgeo.2007.01.022.

Cremaschi, M. (1982), La formazione fluviolacustre del Pleistocene inferiore-medio nel pedappennino emiliano, in *Guida alla geologia del margine appenninico-padano*, edited by G. Cremonini and F. Ricci Lucchi, pp. 145–149, Soc. Geol. Ital., Bologna, Italy.

Daëron, M., J. P. Avouac, and J. Charreau (2007), Modeling the shortening history of a fault tip fold using structural and geomorphic records of deformation, *J. Geophys. Res.*, *112*, B03S13, doi:10.1029/2006JB004460.

Dewey, J. F., M. L. Helman, E. Turco, D. W. H. Hutton, and S. D. Knott (1989), Kinematics of the western Mediterranean, *Alpine Tectonics*, edited by M. P. Coward et al., *Spec. Pub. Geol. Soc. London*, *45*, 265–283.

Di Dio, G., S. Lasagna, D. Preti, and M. Sagne (1997), Stratigrafia dei depositi quaternary della Provincia di Parma, *Boll. Soc. Paleontol. Ital.*, *36*, 179–187.

Di Dio, G., et al. (2005), Carta geologica d'Italia alla scala 1:50,000, Regione Emilia-Romagna, Servizio Geologico, Sismico e dei Suoli, Firenze, Italy.

Dominici, S. (2001), Taphonomy and paleoecology of shallow marine macrofossil assemblages in a collisional setting (late Pliocene-early Pleistocene, western Emilia, Italy), *Palaios*, *16*(4), 336–353.

Duvall, A., E. Kirby, and D. Burbank (2004), Tectonic and lithologic controls on bedrock channel profiles and processes in coastal California, *J. Geophys. Res.*, *109*, F03002, doi:10.1029/2003JF000086.

Eppes, M. C., R. Bierma, F. J. Pazzaglia, and D. Vinson (2008), Soil geomorphology of the Reno Valley, Italy, *Geoderma*, *147*, 97–107.

Erslev, E. A. (1991), Trishear fault-propagation folding, *Geology*, *19*, 617–620, doi:10.1130/0091-7613(1991)019<0617:TFPF>2.3.CO;2.

Fairbanks, R. G., R. A. Mortlock, T. C. Chiu, L. Cao, A. Kaplan, T. P. Guilderson, T. W. Fairbanks, A. L. Bloom, P. M. Grootes, and M. J. Nadeau (2005), Radiocarbon calibration curve spanning 0 to 50,000 years BP based on paired ^{230}Th/^{234}U/^{238}U and ^{14}C dates on pristine corals, *Quat. Sci. Rev.*, *24*, 1781–1796, doi:10.1016/j.quascirev.2005.04.007.

Fischer, M. P., and N. B. Woodward (1992), The geometric evolution of foreland thrust systems, in *Thrust Tectonics*, edited by K. R. McClay, pp. 181–189, Chapman and Hall, London.

Fisher, D. M., and D. J. Anastasio (1994), Kinematic analysis of a large-scale leading edge fold, Lost River Range, Idaho, *J. Struct. Geol.*, *16*, 337–354, doi:10.1016/0191-8141(94)90039-6.

Ford, F., E. A. Williams, A. Artoni, J. Vergés, and S. Hardy (1997), Progressive evolution of a fault-related fold pair from growth strata geometries, Sant Llorenç de Morunys, SE Pyrenees, *J. Struct. Geol.*, *19*, 413–441, doi:10.1016/S0191-8141(96)00116-2.

Gilbert, G. K. (1877), *Report on the Geology of the Henry Mountains*, 160 pp., U.S. Gov. Print. Off., Washington, D. C.

Gold, R. D., E. Cowgill, X. Wang, and X. Chen (2006), Application of trishear fault-propagation folding to active reverse faults: Examples from the Dalong Fault, Gansu Province, NW China, *J. Struct. Geol.*, *28*, 200–219, doi:10.1016/j.jsg.2005.10.006.

Gradstein, F. M., J. G. Ogg, A. G. Smith, W. Bleeker, and L. Lourens (2004), A new geologic time scale, with special reference to Precambrian and Neogene, *Episodes*, *27*(2), 83–100.

Hancock, G. S., and R. S. Anderson (2002), Numerical modeling of fluvial strath-terrace formation in response to oscillating climate, *Geol. Soc. Am. Bull.*, *114*, 1131–1142.

Hardy, S., and J. Poblet (1994), Geometric and numerical model of progressive limb rotation in detachment folds, *Geology*, *22*, 371–374, doi:10.1130/0091-7613(1994)022<0371:GANMOP>2.3.CO;2.

Hardy, S., and J. Poblet (2005), A method for relating fault geometry, slip rate and uplift data above fault-propagation folds, *Basin Res.*, *17*, 417–424, doi:10.1111/j.1365-2117.2005.00268.x.

Hubert-Ferrari, A., J. Suppe, R. Gonzalez-Mieres, and X. Wang (2007), Mechanisms of active folding of the landscape (southern Tian Shan, China), *J. Geophys. Res.*, *112*, B03S09, doi:10.1029/2006JB004362.

Jackson, J., J. F. Ritz, L. Siame, F. Y. Raisbeck, R. Norris, J. Youngson, and E. Bennett (2002), Fault growth and landscape development rates in

Otago, New Zealand, using in situ cosmogenic ^{10}Be, *Earth Planet. Sci. Lett.*, *195*, 185–193, doi:10.1016/S0012-821X(01)00583-0.

Jamison, W. R. (1987), Geometric analysis of fold development in overthrust terranes, *J. Struct. Geol.*, *9*, 207–219, doi:10.1016/0191-8141(87)90026-5.

Kirby, E., and K. Whipple (2001), Quantifying differential rock-uplift rates via stream profile analysis, *Geology*, *29*, 415–418, doi:10.1130/0091-7613(2001)029<0415:QDRURV>2.0.CO;2.

Krzyszkowski, D. (1996), Climatic control on Quaternary fluvial sedimentation in the Kleszczów graben, central Poland, *Quat. Sci. Rev.*, *15*, 315–333, doi:10.1016/0277-3791(95)00040-2.

Lavé, J., and J. P. Avouac (2000), Active folding of fluvial terraces across the Siwaliks Hills, Himalayas of central Nepal, *J. Geophys. Res.*, *105*(B3), 5735–5770, doi:10.1029/1999JB900292.

Mackin, J. H. (1937), Erosional history of the Big Horn Basin, Wyoming, *Geol. Soc. Am. Bull.*, *48*, 813–893.

Malinverno, A., and W. Ryan (1986), Extension in the Tyrrhenian Sea and shortening in the Apennines as result of arc migration driven by sinking of the lithosphere, *Tectonics*, *5*, 227–245, doi:10.1029/TC005i002p00227.

Manzi, V., S. Lugli, F. Ricci Lucchi, and M. Roveri (2005), Deep-water clastic evaporites deposition in the Messinian Adriatic foredeep (northern Apennines, Italy): Did the Mediterranean ever dry out?, *Sedimentology*, *52*, 875–902, doi:10.1111/j.1365-3091.2005.00722.x.

Mary, C., S. Iaccarino, V. Courtillot, J. Besse, and D. M. Aissaohi (1993), Magnetostratigraphy of Pliocene sediments from the Stirone River (Po Valley), *Geophys. J. Int.*, *112*, 359–380, doi:10.1111/j.1365-246X.1993.tb01175.x.

Merritts, D., K. Vincent, and E. Wohl (1994), Long river profiles, tectonism, and eustasy: A guide to interpreting fluvial terraces, *J. Geophys. Res.*, *99*(B7), 14,031–14,050, doi:10.1029/94JB00857.

Meyer, G. A., S. G. Wells, and A. J. T. Jull (1995), Fire and alluvial chronology in Yellowstone National Park: Climate and intrinsic controls on Holocene geomorphic processes, *Geol. Soc. Am. Bull.*, *107*, 1211–1230, doi:10.1130/0016-7606(1995)107<1211:FAACIY>2.3.CO;2.

Mitra, S. (1990), Fault-propagation folds: Geometry, kinematic evolution, and hydrocarbon traps, *AAPG Bull.*, *74*(6), 921–945.

Molnar, P., et al. (1994), Quaternary climate change and the formation of river terraces across growing anticlines on the north flank of the Tien Shan, China, *J. Geol.*, *102*, 583–602.

Mueller, K., and J. Suppe (1997), Growth of Wheeler Ridge anticline, California: Geomorphic evidence for fault-bend folding behaviour during earthquakes, *J. Struct. Geol.*, *19*, 383–396, doi:10.1016/S0191-8141(96)00112-5.

Odin, G. S., F. Ricci Lucchi, F. Tateo, M. Cosca, and J. C. Hunziker (1997), Integrated stratigraphy (biostratigraphy and geochronology) of the early Miocene sequence from the Emilian Apennines (Italy), in *Miocene Stratigraphy an Integrated Approach*, *Dev. Paleontol. Stratigr. Ser.*, vol. 15, edited by A. Montanari et al., pp. 221–247, Elsevier, New York.

Ori, G. G., and P. F. Friend (1984), Sedimentary basins formed and carried piggy-back on active thrust sheets, *Geology*, *12*, 475–478, doi:10.1130/0091-7613(1984)12<475:SBFACP>2.0.CO;2.

Pazzaglia, F. J., and M. T. Brandon (2001), A fluvial record of long-term steady-state uplift and erosion across the Cascadia forearc high, western Washington state, *Am. J. Sci.*, *301*, 385–431, doi:10.2475/ajs.301.4-5.385.

Pazzaglia, F. J., and T. W. Gardner (1993), Fluvial terraces of the lower Susquehanna River, *Geomorphology*, *8*, 83–113, doi:10.1016/0169-555X(93)90031-V.

Pelosio, G., and S. Raffi (1977), Preliminary remarks on mollusk assemblages of the Stirone River Pleistocene series (Parma Province, northern Italy), paper presented at 10th INQUA Congress, pp. 1–19, Quat. Res. Assoc., Birmingham, U. K.

Picotti, V., and F. J. Pazzaglia (2008), A new active tectonic model for the construction of the northern Apennines mountain front near Bologna (Italy), *J. Geophys. Res.*, *113*, B08412, doi:10.1029/2007JB005307.

Picotti, V., R. Capozzi, G. Bertozzi, F. Mosca, A. Sitta, and M. Tornaghi (2007), The Miocene petroleum system of the northern Apennines in the central Po Plain, in *Thrust Belts and Foreland Basins, From Fold Kinematics to Hydrocarbon Systems*, edited by O. Lacombe et al., pp. 117–131, Springer, Berlin.

Pieri, M. (1983), Three seismic profiles through the Po Plain, in *Seismic Expression of Structural Styles*, *AAPG Stud. Geol. Ser.*, vol. 15, edited by A. W. Bally, pp. 8–26, Am. Assoc. of Pet. Geol., Tulsa, Okla.

Pieri, M. (1992), Cortemaggiore Field-Italy Po Plain, northern Apennines, in *Structural Traps VII, Treatise of Petroleum Geology, Atlas of Oil and Gas Fields*, edited by E. A. Beaumont and N. H. Foster, pp. 99–118, Am. Assoc. of Pet. Geol., Tulsa, Okla.

Pieri, M., and L. Mattavelli (1986), Geologic framework of Italian petroleum resources, *AAPG Bull.*, *70*(2), 103–130.

Pini, G. A. (1999), Tectonosomes and olistrostromes in the argille scagliose of the northern Apennines, Italy, *Spec. Pap. Geol. Soc. Am.*, *335*, 70 pp.

Rafini, S., and E. Mercier (2002), Forward modelling of foreland basins progressive unconformities, *Sediment. Geol.*, *146*, 75–89, doi:10.1016/S0037-0738(01)00167-1.

Riba, O. (1976), Syntectonic unconformities of the Alto Cardener, Spanish Pyrenees: A genetic interpretation, *Sediment. Geol.*, *15*, 213–233, doi:10.1016/0037-0738(76)90017-8.

Ricci Lucchi, F. (1975), Miocene paleogeograpy and basin analysis in the periadriatic Apennines, in *Geology of Italy*, edited by C. Squyres, pp. 5–111, Pet. Explor. Soc. of Libya, Tripoli.

Ricci Lucchi, F. (1986), The Oligocene to recent foreland basins of the northern Apennines, in *Foreland Basins*, edited by P. A. Allen and P. Homewood, pp. 105–140, Blackwell, Freiburg, Germany.

Rockwell, T. K., E. A. Keller, M. N. Clark, and D. L. Johnson (1984), Chronology and rates of faulting of Ventura River terraces, California, *Geol. Soc. Am. Bull.*, *95*, 1466–1474, doi:10.1130/0016-7606(1984)95<1466:CAROFO>2.0.CO;2.

Rockwell, T. K., E. A. Keller, and G. R. Dembroff (1988), Quaternary rate of folding of the Ventura Avenue anticline, western Transverse Ranges, southern California, *Geol. Soc. Am. Bull.*, *100*, 850–858, doi:10.1130/0016-7606(1988)100<0850:QROFOT>2.3.CO;2.

Rosenbaum, G., and G. S. Lister (2004), Neogene and Quaternary rollback evolution of the Tyrrhenian Sea, the Apennines, and the Sicilian Maghrebides, *Tectonics*, *23*, TC1013, doi:10.1029/2003TC001518.

Roveri, M., and M. Taviani (2003), Calcarenite and sapropel deposition in the Mediterranean Pliocene: Shallow- and deep-water record of astronomically driven climatic events, *Terra Nova*, *15*(4), 279–286, doi:10.1046/j.1365-3121.2003.00492.x.

Scharer, K. M., D. W. Burbank, J. Chen, and R. J. Weldon (2006), Kinematic models of fluvial terraces over active detachment folds: Constraints on the growth mechanism of the Kashi-Atushi fold system, Chinese Tian Shan, *Geol. Soc. Am. Bull.*, *118*, 1006–1021, doi:10.1130/B25835.1.

Schumm, S. A. (1969), River metamorphosis, *J. Hydraul. Div. Am. Soc. Civ. Eng.*, *95*, 255–273.

Simoes, M., J. P. Avouac, Y. G. Chen, A. K. Singhvi, C. Y. Wang, M. Jaiswal, Y. C. Chan, and S. Bernard (2007), Kinematic analysis of the Pakuashan fault tip fold, west central Taiwan: Shortening rate and age of folding inception, *J. Geophys. Res.*, *112*, B03S14, doi:10.1029/2005JB004198.

Simpson, G. (2004), Role of river incision in enhancing deformation, *Geology*, *32*, 341–344, doi:10.1130/G20190.2.

Snyder, N. P., K. X. Whipple, G. E. Tucker, and D. J. Merritts (2000), Landscape response to tectonic forcing: Digital elevation model analysis of stream profiles in the Mendocino triple junction region, northern Califronia, *Geol. Soc. Am. Bull.*, *112*, 1250–1263, doi:10.1130/0016-7606(2000)112<1250:LRTTFD>2.3.CO;2.

Spagnolo, M., and F. J. Pazzaglia (2005), Testing the geological influences on the evolution of river profiles: A case from the northern Apennines, Italy, *Geogr. Fis. Din. Quaternaria*, *28*, 103–113.

Storti, F., and J. Poblet (1997), Growth stratal architectures associated to décollement folds and fault-propagation folds; inferences on fold kinematics, *Tectonophysics*, *282*(1–4), 353–373, doi:10.1016/S0040-1951(97)00230-8.

Suppe, J. (1983), Geometry and kinematics of fault-bend folding, *Am. J. Sci.*, *283*, 684–721.

Suppe, J. (1985), *Principles of Structural Geology*, 537 pp., Prentice-Hall, Englewood Cliffs, N. J.

Suppe, J., and D. A. Medwedeff (1990), Geometry and kinematics of fault-propagation folding, *Eclogae Geol. Helv.*, *83*, 409–454.

Suppe, J., G. T. Chou, and S. C. Hook (1992), Rates of folding and faulting determined from growth strata, in *Thrust Tectonics*, edited by K. R. McClay, pp. 105–121, Chapman and Hall, London.

Suppe, J., F. Sabat, J. A. Muñoz, J. Poblet, E. Roca, and J. Vergés (1997), Bed-by-bed fold growth by kink-band migration: Sant Llorenç de Morunys, eastern Pyrenees, *J. Struct. Geol.*, *19*, 443–461, doi:10.1016/S0191-8141(96)00103-4.

Tavani, S., F. Storti, and F. Salvini (2006), Double-edge fault-propagation folding: Geometry and kinematics, *J. Struct. Geol.*, *28*, 19–35, doi:10.1016/j.jsg.2005.09.007.

Thompson, S. C., R. J. Weldon, C. M. Rubin, K. Abdrakhmatov, P. Molnar, and G. W. Berger (2002), Late Quaternary slip rates across the central Tien Shan, Kyrgyzstan, central Asia, *J. Geophys. Res.*, *107*(B9), 2203, doi:10.1029/2001JB000596.

Vergés, J., D. Burbank, and A. Meigs (1996), Unfolding: An inverse approach to fold kinematics, *Geology*, *24*, 175–178, doi:10.1130/0091-7613(1996)024<0175:UAIATF>2.3.CO;2.

Wegmann, K. W., and F. J. Pazzaglia (2002), Holocene strath terraces, climate change, and active tectonics; the Clearwater River basin, Olympic

Peninsula, Washington State, *Geol. Soc. Am. Bull.*, *114*, 731–744, doi:10.1130/0016-7606(2002)114<0731:HSTCCA>2.0.CO;2.

Wegmann, K. W., and F. J. Pazzaglia (2009), Late Quaternary fluvial terraces of the Romagna and Marche Apennines, Italy: Climatic, lithologic, and tectonic controls on terrace genesis in an active orogen, *Quat. Sci. Rev.*, *28*, 137–165.

Woodward, N. B. (1997), Low-amplitude evolution of break-thrust folding, *J. Struct. Geol.*, *19*, 293–301, doi:10.1016/S0191-8141(96)00102-2.

Zapata, T. R., and R. W. Allmendinger (1996), Growth strata record of instantaneous and progressive limb rotation, Precordillera thrust belt and Bermejo Basin, Argentina, *Tectonics*, *15*, 1065–1083, doi:10.1029/96TC00431.

Zaprowski, B. J., F. J. Pazzaglia, and E. B. Evenson (2005), Climatic influences on profile concavity and river incision, *J. Geophys. Res.*, *110*, F03004, doi:10.1029/2004JF000138.

Zattin, M., V. Picotti, and G. G. Zuffa (2002), Fission-track reconstruction of the front of the northern Apennine thrust wedge and overlying Ligurian unit, *Am. J. Sci.*, *302*, 346–379, doi:10.2475/ajs.302.4.346.

D. J. Anastasio and F. J. Pazzaglia, Department of Earth and Environmental Sciences, Lehigh University, Bethlehem, PA 18015, USA.

L. F. Wilson, ExxonMobil Exploration Company, Houston, TX 77210, USA. (luke.f.wilson@exxonmobile.com)